WATER RESOURCES CENTER RESEARCH REPORT NUMBER 206

PHOTOLYTIC OZONATION FOR PROTECTION AND REHABILITATION OF GROUND-WATER RESOURCES; A MECHANISTIC STUDY

By Gary R. Peyton, Michelle A. Smith, and Brent M. Peyton

Aquatic Chemistry Section
Illinois State Water Survey
Champaign, Illinois 61820

REPORT
PROJECT NO. S-104-ILL

UNIVERSITY OF ILLINOIS
WATER RESOURCE CENTER
2535 Hydrosystems Laboratory
Urbana, Illinois 61801

January 1987

TABLE OF CONTENTS

LIST OF TABLES

LIST OF FIGURES

ABSTRACT

The cleanup of ground-water resources which have been contaminated by anthropogenic organic compounds is difficult and expensive. Furthermore, most treatment methods merely transfer the contaminant to another phase, such as an adsorbant or the atmosphere. A treatment process which produces harmless by-products, could be set up on-site, and does not require the transport of hazardous materials is very desirable for such cleanup operations. Photolytic ozonation, the combination of ozone treatment and ultraviolet irradiation, is an oxidative water treatment process which is capable of converting virtually any organic pollutant completely to carbon dioxide and water. Thus, it is potentially a very "clean" solution to many contamination problems. There has, however, been disagreement in the scientific literature concerning the effectiveness of the process, due largely to a lack of understanding of the chemistry which is involved.

In this project, photolytic ozonation was studied at the laboratory scale, to better understand and, if possible, model the complex chemical reaction mechanism, so that the process can be more easily optimized from an economic standpoint. It was shown that hydroxyl radical, the active species responsible for the destruction of organic pollutants, is not generated directly by ozone photolysis as has generally been speculated, but is produced by secondary reactions.

A model has been developed which explains the behavior of the process under a variety of conditions and is useful for the prediction of process performance. The model includes parameters, the values of which may be inferred from the chemical structure of the organic pollutant. The reaction system is seen to be "versatile" in that it has alternate pathways by which pollutant destruction may proceed, depending on conditions in the water being treated.

Gary R. Peyton, Michelle A. Smith, and Brent M. Peyton

PHOTOLYTIC OZONATION FOR PROTECTION AND REHABILITATION OF GROUND-WATER RESOURCES; A MECHANISTIC STUDY

Water Resource Center Research Report 206, 58 pp.

Keywords: Ozone, ground-water, photolysis, ozonation, hydrogen peroxide, oxidation, hydroxyl radical, water treatment

SECTION 1

INTRODUCTION

RESEARCH NEED

The cleanup of ground-water resources which have been contaminated by anthropogenic organic compounds is difficult and expensive. Furthermore, most treatment methods merely transfer the contaminant to another phase, such as an adsorbent or the atmosphere. A treatment process which produces harmless by-products, could be set up on-site, and does not require the transport of hazardous materials is very desirable for such cleanup operations. A process known as photolytic ozonation (1-4) provides "absolute" treatment for organics in water, having the power to oxidize organic compounds completely to carbon dioxide and water while "mineralizing" organic chlorine to chloride, organic sulfur to sulfate, etc. Although the power of photolytic ozonation has been known for some time (5-6), the chemical details of this process have not been well understood, so that the empirical application of the process has in some cases led to disappointing or conflicting results between investigators.

The research which was needed in this area consisted of two parts: (1) the fundamental mechanistic study of photolytic ozonation in order to understand and control reaction conditions for optimum treatment efficiency, and (2) suitable modeling of the mass transfer/chemical reaction/photochemical reaction interplay in order to provide design criteria for actual treatment installations. This information obtained in this study will aid chemists and engineers in estimating the efficacy of treatment of a given water from its composition, by knowing how the constituent solutes interact with the treatment chemistry. It also provides design criteria for application of photolytic ozonation in field trials for on-site aquifer rehabilitation, leachate treatment, and solid waste or excavation extract destruction. The ultimate benefactor is of course the public, through the increased ability to protect and reclaim our water resources.

NATURE, SCOPE, AND OBJECTIVES OF THE RESEARCH

Photolytic ozonation is a process in which ozone is passed through water which is being irradiated with ultraviolet (UV) light. The UV light causes photolysis of the dissolved ozone to yield species which are much more reactive than ozone itself. Among these free radical species is hydroxyl radical, •OH, which is capable of abstracting a hydrogen atom from virtually any carbon-hydrogen bond, thus initiating the stepwise destruction of otherwise quite refractory organic compounds. The chemical processes which follow ozone photolysis are quite complex, involving between twenty and thirty chemical reactions between oxygen and hydrogen species alone (4).

Photolytic ozonation is in many ways more suitable for treatment of contaminated water than is incineration. It is easier to control and monitor, and therefore potentially more complete in the destruction of organic compounds. The methods are easily adaptable to on-site treatment in mobile units, and the nonphotolytic variant (ozone/hydrogen peroxide) may find limited application to in situ aquifer reclamation. Other than perhaps oxygen, no reagents must be transported to the site, while the ultimate by-products are carbon dioxide and water.

In this project a laboratory study of the chemical reaction mechanism was performed using a laboratory scale continually-sparged stirred tank photochemical reactor (CSTPR). Both the reaction conditions and the model substance being destroyed were varied in order to study the effect of process parameters on the efficiency of the treatment process. The dynamics of the reaction (mass transfer with chemical and photochemical reaction) was also studied at the laboratory scale using the CSTPR.

The objectives of the proposed research were:

1) To obtain a better understanding, at the mechanistic level, of photolytic ozonation as applied to the destruction of organic pollutants in ground water;

2) To investigate and model the interaction between mass transfer, chemical reaction and photochemical reaction which occurs in this system, as a function of ozone dose rate, UV intensity, solution composition, and reactor configuration.

RELATED RESEARCH

The Mechanism of Photolytic Ozonation

Photolytic ozonation is the UV-irradiation of a solution containing or in contact with ozone. This process, first developed in the early seventies for destruction of cyanide complexes (5), was soon found to be effective for destruction of organic compounds in water (1-4, 6-12). During the period between 1975 and 1980, there was considerable speculation in the literature concerning the mechanism of photolytic ozonation, but little evidence was available to confirm or refute this speculation.

Also during this period, considerable disparity was found between the results of various groups as to the increased effectiveness of photolytic ozonation over ozonation alone (6,10). Studies (1) conducted by this investigator for USEPA during the period 1977-1980 on dilute ($\leq$100 µg/L) organics in water indicated a complex free radical reaction mechanism with stoichiometric efficiencies which were quite dependent on UV intensity and substrate concentration, as well as ozone dose rate. These indications were in agreement with the results of Taube (13), who found the production of hydrogen peroxide upon ozone photolysis in aqueous acetic acid solution. Taube and Bray had shown earlier (14) that in acidic solution, ozone and hydrogen peroxide reacted in a chain system in which hydroperoxyl ($HO_2\cdot$) and hydroxyl ($\cdot OH$) radicals were produced. The results of Baxendale and Wilson (15), who studied the photolysis of aqueous hydrogen peroxide in the presence of various organic compounds including acetic acid, left it unclear, however, whether the photolysis of aqueous ozone in Taube's work resulted directly in the production of hydrogen peroxide or indirectly, through the action of hydroxyl radical upon acetic acid.

Although no mechanistic studies were included in the above EPA project, the results were promising enough in terms of organic compound removal that USEPA funded a three-year follow-up pilot study of the process for trihalomethane precursor removal in drinking water. In addition to the pilot-scale investigation, an abbreviated laboratory study was also included with the goal of better understanding the process and perhaps identifying the active species. The results of that study

(4,16,17) provided kinetic evidence that ozone photolysis at 2537$\mathring{A}$ in aqueous solution yields peroxide (eq. 1), followed by reaction of the conjugate base, hydroperoxy anion (HO_2^-), with ozone to yield superoxide[1] ($\cdot O_2^-$)

$$O_3 + H_2O \xrightarrow{h\nu} O_2 + H_2O_2 \quad (1)$$

$$H_2O_2 + H_2O \rightleftharpoons H_3O^+ + HO_2^- \quad (2)$$

$$O_3 + HO_2^- \rightarrow O_2 + \cdot O_2^- + \cdot OH \quad (3)$$

$$O_3 + \cdot O_2^- + H_2O \rightarrow 2O_2 + {}^-OH + \cdot OH \quad (4)$$

and hydroxyl radical (eq. 3). This initiation sequence will be called Scheme I. Superoxide, in turn, reacts with ozone to yield hydroxyl radical (eq. 4). As will be seen in a later section, this "reaction" is actually a multi-step process involving the production and protonation of ozonide ion followed by decay of HO_3. In the absence of organic compounds, equations 3 and 4 plus equation 5, simply represent the chain photodecomposition of ozone with initiation steps 1 and 2.

$$O_3 + \cdot OH + H_2O \rightarrow O_2 + H_3O^+ + \cdot O_2^- \quad (5)$$

When no organic compounds are present to scavenge hydroxyl radical, this reaction proceeds with very high quantum yield. However, in the presence of excess ($\geq 10^{-4}$ M) organic compound containing an abstractable hydrogen atom,

$$\cdot OH + RH \rightarrow H_2O + R\cdot \quad , \quad (6)$$

which occurs at diffusion controlled rates for many organic compounds (18). This is followed by reaction between R$\cdot$ and dioxygen to give organic peroxy radicals

---

[1]For simplicity, the $HO_2\cdot/\cdot O_2^-$ conjugate pair has been represented as $\cdot O_2^-$, as when pH $\geq pK_a$.

$$R\cdot + O_2 \rightarrow RO_2\cdot \qquad (7)$$

which can photolyze, disproportionate to more stable molecules, or regenerate further superoxide, which reenters the system by reaction with ozone via equation 4. Repetition of the above process leads ultimately to complete organic compound destruction. Consideration of the above model of the reaction system indicates how varying the reaction conditions (ozone dose rate, UV intensity, substrate concentration) can greatly affect the efficiency of the process, particularly in systems where there is a competing reaction between ozone and organic compound. The complexity of this mechanistic pathway is thus consistent with the varying results which have been reported in the literature. This prototype mechanism has been reported previously (16,17) and is presented diagrammatically in Figure 1.

An alternative pathway (Scheme II) begins with an initiation step which is analogous to that found in the gas phase in the presence of water, where ozone photolysis at 2537Å produces $O(^1D)$ (eq. 8), which reacts immediately with water to produce two hydroxyl radicals (eq. 9).

$$O_3 \xrightarrow[\lambda = 2537\text{Å}]{h\nu} O_2 + O(^1D) \qquad (8)$$

$$O(^1D) + H_2O \rightarrow 2\cdot OH \qquad (9)$$

In the gas phase, "immediately" means within the first few collisions, while in the condensed phase the solvation sphere is water, and $O(^1D)$ if it occurs, probably reacts by insertion into the O-H bond. Reactions 4 and 5 follow, again completing the chain system. This is the mechanism which has been most frequently speculated in the literature, probably because these gas-phase reactions have been known for some time in the atmospheric chemistry literature.

Several important differences can be seen between Schemes I and II which could greatly affect the engineering of actual treatment systems. The active specie primarily responsible for organic compound destruction is in both cases hydroxyl radical. In Scheme I hydroxyl radical is produced by secondary reactions involving further reactions with ozone, while

in Scheme II it is produced essentially by the photolysis step. Therefore, in Scheme I "overphotolysis" of the ozone, i.e. photolysis of too great a fraction of the ozone may not leave enough ozone for the maximum possible occurrence of secondary hydroxyl-producing reactions, while "underphotolysis" may not utilize the ozone completely for hydroxyl radical production. On the other hand, the maximum ·OH yield in Scheme II is realized when all the ozone is photolyzed, requiring considerably more UV input, since absorbance decreases with decreasing concentration.

If scheme I is the correct mechanism, it can be seen that the same effect should be obtainable by the use of ozone in combination with hydrogen peroxide. However, the ozone/peroxide system has shortcomings. The amount of peroxide must be carefully matched to the ozone dose or underutilization of one reagent will result. If a large excess of peroxide is used, it can actually compete with substrate for hydroxyl radical. Nonetheless, there are treatment situations, such as high UV absorbance by the waste stream in which O_3/H_2O_2 might be preferable to O_3/UV. In any case, it is important to demonstrate the equivalence or non-equivalence of these two reaction systems.

Consideration of the rate constants in the ozone/UV system shows that for Scheme I there should be a wide range of UV intensities for which the secondary reaction rates are fast enough to "self-regulate" the stoichiometry of the system. That is, a wide range of UV intensities can be tolerated before "overphotolysis" occurs.

Several features of the previous studies (4,16,17) prevent definitive mechanistic conclusions from being drawn:

1) There was no data collected for ozone content in the off-gas during the laboratory study. Ozone mass balance data is essential to the arguments required to distinguish between mechanisms.

2) Because of the scope of the EPA-sponsored project (4), the substrate in the pilot study was the trihalomethane formation potential of the natural humic material present in the river water used. Since THMFP is a property of the humic macromolecules rather than a specie itself, no quantitative stoichiometric conclusions can be drawn concerning organic removal.

3) Only a limited range of UV intensities was used and it was not possible to determine the dependence of process efficiency on UV power.

4) In general, the scope of the EPA-sponsored project did not include a thorough mechanistic study.

The overall goal of the present project was to gain a better understanding of the reaction mechanism and dynamics so that useful predictions for optimum configuration and process performance could be made. To achieve this goal required a great number of experiments under a diverse set of experimental conditions, more thorough analytical chemistry and experimental control, and a more comprehensive kinetic and mechanistic analysis than had been performed in previous studies. Through these studies the mechanism of photolytic ozonation has been elucidated, and a predictive tool has been developed which will be useful in the application of the process to actual water treatment situations.

SECTION 2

EXPERIMENTAL

REACTOR SYSTEM

The reactor was a Continuously-sparged Stirred Tank Photochemical Reactor (CSTPR), with standard relative dimensions (19,20) and four quartz lamp wells mounted in the quadrants created by the baffles (20). The reactor body (10.65 L total volume, 8.5 L liquid volume) was made from a piece of Corning Pyrex(R) process pipe, 12" tall, with a nominal i.d. of 9". The reactor heads were machined from 1/2" thick sheet Teflon(R), as were the baffles, sparger, six-blade impeller, and o-ring glands to secure the lamp wells. The stirring gland was glass (Cole-Parmer, Chicago, IL) with a PTFE-coated Viton o-ring seal, and glass shaft. The impeller was pinned through a hole bored in the glass shaft, using a PTFE pin. The stirring motor was a 1/8 hp, variable speed DC motor with SCR controller (W. W. Grainger, Decatur, IL), the speed of which was set using a photo-tachometer. Gas fittings and liquid sample valve were PTFE as was all connecting tubing. All wetted surfaces were either PTFE or glass.

Ozone was generated from dry oxygen using a Grace model LG-2-L2 ozone generator. Inlet and off gas flows were regulated to within 0.1% full scale (usually 1% of the measured value) by two UFC-1000 mass flow controllers attached to a URS-100 power supply and digital readout (Unit Instruments, Inc., Orange, CA). This system can respond quickly to a reactor pressure change (such as that caused by switching the ozone monitor from feed gas to off gas), restoring the flow rate to within ±2% of the set point in a period of 2-4 seconds. Ozone concentration was followed by a PCI high-concentration (model HC) ozone monitor which gave digital readout as well as providing an analog signal to a strip-chart recorder for later calculation of ozone doses. Factory calibration of

this monitor was checked by wet chemical methods for ozone analysis (described below) by bubbling ozone into the CSTPR and withdrawing samples as a function of time.

The reactor and manifold system used are shown in Figure 2. The ozone stream from the ozone generator (OG) is split and sent to two mass flow controllers (MFC). The stream through MFC_2 may either be sent as feed to the reactor (R) or bypassed to the vent (V) using Teflon(R) solenoid valve V_c, as was done during generator warm-up and initial concentration adjustment. The slip stream through MFC_1 to V_a is diverted through V_a and V_b to the ozone monitor (OM) for feed gas concentration measurement or sent to vent. Total gas flow through the ozone generator is kept constant since it is the sum of the flows through the two mass flow controllers MFC_1, and MFC_2. Off gas from the reactor is kept at constant pressure using the back pressure column (BPC) which doubles as a crude ozone kill unit. The back pressure is sufficient to force off gas through the ozone monitor when V_b is appropriately positioned. The mass flow controllers (which see only dry gas), the back pressure column (downstream of the system) and the spectrophotometric cell in the ozone monitor are the only components made of materials other than PTFE or glass, since severe decomposition of ozone by stainless steel tubing was noted in previous work (4).

The G10T5-1/2 ultraviolet lamps (American Ultraviolet, Chatham, N.J.) were rated at 5-1/2 W of UV power at 100 hrs. life. Lamp intensities were measured both radiometrically and actinometrically (described below) and were found to differ considerably from those specifications. In the course of this work, from 1/4 to 3-1/2 lamps were used in an experiment. Fractional lamp values were obtained by using a foil shroud on the lamps.

No attempt was made to optimize reaction conditions or mass transfer during this study. Conditions were chosen to favor precise and accurate data collection for mechanistic determination.

ANALYTICAL METHODS

Oxidant Analysis

Ozone in the aqueous phase was analyzed by the indigo method of Bader and Hoigne (21,22), using the disulfonate rather than the trisulfonate as originally described by those authors. This method (hereafter called the HBI method) was calibrated in purified water against the iodimetric method of Flamm (23) ("BKI" method) and checked by UV absorbance using the extinction coefficient of Hart et al. (24). The iodimetric method was, itself, calibrated by quantitative iodine liberation using excess iodide and standard iodate solution, prepared using dried potassium iodate as a primary standard. Ozone in the gas phase was measured by UV absorbance, with the factory calibration checked against the wet methods by absorbing the gas in reagent solution contained in the reactor.

Hydrogen peroxide was measured colorimetrically by complexation with Ti(IV) ("TI4" method) (25) or by the method of Masschelein et al. (26) (MDL method). As ozone appears to interfere negatively with hydrogen peroxide measurement using the TI4 method, ozone was quickly and vigorously sparged from solution with oxygen before peroxide measurements were made. The MDL method was not used on ozone-containing solutions. Total oxidants were measured iodimetrically by the method of Flamm (23), but with the addition of a small quantity of ammonium molybdate to catalyze the reaction with peroxides (BKI/M method).

Organic Analysis

Methanol and t-butanol were quantitatively measured by direct aqueous injection gas chromatography with flame ionization detection, using either a Chromosorb 102 or 105 column. Column lengths and temperatures were not critical since only one product peak was detected (which did not interfere with analysis) during the entire study. Formaldehyde was determined using the chromotropic acid method of Houle, et al. (27). Formic acid analysis was by the method of Bethge and Lindstrom (28) in

which the benzyl ester is analyzed by glc on a 6' x 1/8" SP-1000 (Supelco, Inc., Bellefonte, PA) or FFAP column. Identity of analyte peaks was verified by GC/MS.

UV Lamp Intensity

Ultraviolet output from the lamps was measured by actinometry and radiometry. Radiometric measurement was made using a model IL700A Research Radiometer (International Light, Inc., Newburyport, Mass.) as a function of distance along the lamp (i.e. parallel to the cylindrical symmetry axis, of the lamp) for several different radial distances from the central lamp axis, both with and without a 254 nm bandpass filter. The intensity profile thus obtained was integrated over the surface of rotation to obtain an estimate of the total flux from the lamp. Measurements at three different distances yielded an integrated value of the total flux, after correction for attenuation by the quartz lamp well, of 0.94 ± 0.03 W, which corresponds to 1.4×10^{-5} Einstein/L•min at 254 nm.

Actinometric measurement was by the method of Parker (29), employing the optically dense actinometer potassium ferrioxalate. Since this actinometer also responds in the visible region, the value was corrected by the ratio of 254 nm to total radiation as measured by the radiometer, resulting in a value 40% higher for the actinometric compared to the radiometric measurement. Because of this uncertainty, the radiometric values have been used in all calculations because of the selectivity of the radiometer when used with the 254 nm band pass filter.

Reagents

All chemicals were reagent grade, and were used without further purification. Deionized water was used in all experiments. When a buffer was used, it was made up to 0.015 M in total phosphate using either salts or phosphoric acid and freshly prepared sodium hydroxide solution.

SECTION 3

THEORETICAL MODEL FOR THE OZONE/HYDROGEN PEROXIDE/UV SYSTEM

The model for photolytic ozonation/peroxidation (POP) which was developed during this study is derived from a simpler version, published earlier (4,16,17), which was based on the finding that hydrogen peroxide was the direct product of ozone photolysis (4). That early model, described in Section 1, was qualitative in nature, however, and one objective of the present study was the formulation of a quantitative model which would be useful in the design of treatment units.

The mechanism of POP is complex because most of the species involved are free radicals and therefore almost all react with one another. Addition of an organic compound to the system introduces additional reactions by means of the free radical reaction products of the parent compound as well as those of intermediate by-products. The literature was surveyed to locate as many of the reaction rate constants as were available. These bimolecular rate constants are given in Table 1 for the oxygen/hydrogen species and for selected organic molecules and radicals. Previous studies (4) had shown that the complete system of rate equations was not amenable to direct solution, due to the importance of terms which were a small difference between two inaccurately-known large numbers. However, comparison of numerical values of terms in the rate expressions was sufficient to allow selection of the most important reactions for inclusion in the model.

The important reactions were then written in the form of a flow chart and mass-balance equations written for each species. This flow chart is shown in Figures 3 and 4 for the two candidate mechanisms under consideration. Figure 3 shows Case I, in which aqueous ozone photolysis produces hydrogen peroxide, which then dissociates as a weak acid with pK_a = 11.6 (30). The conjugate base of hydrogen peroxide (HO_2^-) reacts with ozone (31) to form ozonide ion (O_3^-), which protonates (pk_a = 6.15, reference 32) to HO_3. That species, in turn, decomposes to dioxygen (O_2) and hydroxyl radical (OH), the primary active species. Hydroxyl radical reacts with aliphatic organic compounds (denoted by HRH in Figures 3

and 4) by abstracting a hydrogen atom to give the organic free radical $\cdot RH$, which quickly reacts with dioxygen to form the organic peroxy radical $\cdot O_2RH$ (33,34). This radical decomposes by both first and second order processes (35). The former yields superoxide (O_2^-) while the latter produces hydrogen peroxide by reactions which are not yet well understood. Finally, superoxide reacts very quickly with ozone in solution to close the chain reaction shown in Figure 3.

Figure 4 shows the flow chart which results from case II, in which photolysis of aqueous ozone produces two hydroxyl radicals. Since these radicals react directly with organic substrate, hydrogen peroxide, if present, must be produced either by the secondary reactions of peroxy radicals (35) or disproportionation of superoxide and/or $HO_2\cdot$ (36). The latter reaction can be demonstrated on the basis of literature rate constants to be unimportant in both schemes above a pH of about 3.7, due to the rapid reaction of superoxide with ozone. That reaction is therefore not shown in Figures 3 or 4 which include only important reactions. This simplification is necessary to reduce the number of variables in the mass balance equations to a manageable level, but all known omissions can be justified on the basis of kinetic arguments similar to those above.

In Figures 3 and 4, and in the equations which follow, the large letters D_u, A_O, A_H, R represent the measurable quantities of incoming ozone dose rate, accumulation rates of ozone and hydrogen peroxide, respectively, and the reaction rate of parent compound. Greek letters α, β, γ, and δ denote the efficiency with which each of the steps takes place. By this means, the competition of side reactions can be included without the knowledge of the specific reactions which would be required for explicit inclusion in the flow diagram. More specifically, α is the efficiency with which ozonide ion is converted to hydroxyl radical, and β is the efficiency with which all hydroxyl radical reacts with the organic compound of interest. The efficiency of production of superoxide from organic radical is γ, while the extent to which remaining $\cdot O_2RH$ reacts to produce hydrogen peroxide is δ for $\cdot O_2RH$ disappearance and $\delta/2$ for H_2O_2 production. Accumulation of free radical intermediates may be neglected, since it can be shown by kinetic considerations that their concentrations

(and thus accumulation rates) remain very low. This assumption is equivalent to the usual steady-state approximation in chemical kinetics (37) and in fact the mass-balance relationships are analogous to the expressions which could be derived from the rate equations using the steady-state approximation.

The mass-balance relationships may also be interpreted in another manner. Instead of representing the instantaneous rates of the various processes, the upper and lower case symbols may be interpreted to represent the extent of reaction, that is, the rates, integrated from the start of the reaction to time t. Thus, R(t) is just the total amount of substrate removed up to time t, Du(t) the total amount of ozone utilized up to time t, etc. While the reaction rate interpretation is useful for confirmation of the proposed mechanism and interpreting shifts from one mechanism to another during the course of the reaction, the integrated form is the most useful for studying the effect of process variables on the efficiency of destruction of organic compounds. Since both forms will be used, care will be taken to distinguish between them in the text.

The mass balance expressions for the species or conjugate pairs O_3, $H_2O_2 \rightleftarrows HO_2^-$, HRH, and $HO_2 \rightleftarrows O_2^-$, were written in terms of quantities which were measurables in the laboratory (capital letters), rates which were not directly measurable (lower case letters) and efficiencies (greek letters). The system of equations which resulted was solved to eliminate the unknown rates and obtain an expression which resembles an overall destruction efficiency in the sense that it contains the disappearance rate of organic compound in the numerator and the consumption rate of ozone (corrected for the accumulation of oxidants) in the denominator. For case I this expression is given by equation 10, where $\varepsilon_d{}^I$ is defined as the "destruction efficiency" for case I.

$$\varepsilon_d{}^I = \frac{R_T}{D_u - A_O - A_H + P_H(3\alpha^{-1} - 1)} = \frac{2}{3(\gamma\beta)^{-1} - \gamma - (1 - \gamma)\delta} \qquad (10)$$

Inspection of Figure 3 reveals that there are four mass balance equations and four unknowns (a, b, g, and h). Thus, one cannot eliminate all of the unknowns from this set of equation unless some additional means of evaluating one of the unknowns is available. This was done by evaluating $h = P_H$, the hydrogen peroxide photolysis rate, from separate experiments, as described in Section 4.

A similar flow chart for Case II is shown in Figure 4. The difference between Case II and Case I is that in Case II, photolysis of aqueous ozone is assumed to directly produce two hydroxyl radicals, as in the gas phase. The resulting "efficiency" expression is given by equation 11.

$$\varepsilon_d^{II} \equiv \frac{R_T}{D_u - A_O + A_H\,(2 - \alpha) + P_H\,(3 - \alpha)} = \frac{2}{[1/\beta + (2 - \alpha)(\gamma + (1 - \gamma)\delta)]} \qquad (11)$$

Expressions similar to equations 10 and 11 were derived for systems in which disappearance only of parent compound was measured. In these instances it is necessary to use a modified model in which active species (e.g. superoxide) feedback from hydroxyl radical reactions with by-products is included. This expression is not derived here, but is discussed briefly in a later section.

Wherever possible, experiments were designed to permit estimation of some of the individual step efficiencies: α, β, γ, and δ. The value of the quantity β is close to unity early in the reaction when products have not had time to accumulate. Later in the experiment it should have a value of

$$\beta = \frac{k_1[HRH][OH]}{\Sigma_i k_i[C_i][OH]} \qquad (12)$$

later in the experiment. As long as the concentration of organic compounds is considerably larger than that of ozone, the C_i are simply the concentrations of parent compound and organic reaction products, since the rate constant for reaction of H_2O_2 with OH is about 1-1/2 to 2 orders of

magnitude lower than for reaction of OH with organic compounds (see Table 1). In addition, hydroxyl radical rate constants for reaction with organic compounds tend to be similar in magnitude at about $k = 10^8 - 10^9\ M^{-1}\ s^{-1}$. Therefore, a first approximation which is sometimes useful is

$$\beta = \frac{[HRH]}{\Sigma_i[Ci]} \cong \frac{[HRH]}{[HRH]_o} \quad , \tag{13}$$

where $[HRH]_o$ is the initial HRH concentration. This approximation is most accurate when fragmentation of the organic molecule to produce a greater total number of organic molecules has not occurred. In general, the hydrogen abstraction reactions of OH have the effect of "nibbling at the edges" of aliphatic organic molecules, with fragmentation kept to a minimum.

Other experimental conditions were picked to aid evaluation of the model. Parent compounds were chosen which would not undergo direct ozonolysis reactions. Methanol was chosen for that reason as well as for the fact that decomposition of the oxygen adduct of its free radical to yield superoxide is well known (33), and that its stable reaction products are known and relatively easy to quantitate. Thus, a value of Υ close to unity is expected for methanol. Tertiary butyl alcohol was chosen as an example of a compound for which $\Upsilon \cong o$, since there is no structurally convenient way for a proton to leave its oxygen adduct, the peroxyl radical

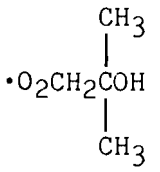

This fact prevents the direct formation of superoxide and allows the self-reaction of its peroxyl radical to yield hydrogen peroxide. Thus, the parameter Υ can, to a first approximation, be derived from a consideration of the structural properties of the molecule being treated.

Less is known about the efficiency parameter α. For α to be less than one, either O_3^- or HO_3 would have to undergo side reactions with other species present in solution. There is little knowledge about the chemistry of ozonide from which to predict such side reactions. Therefore, values of alpha were determined from the model in situations where β and Υ could be experimentally well defined.

The parameter δ is not important for molecules with large Υ, such as methanol. It becomes important for molecules with small Υ (i.e. t-butanol), as it represents the active species feedback cycle by regenerating hydrogen peroxide. This regeneration can be quite efficient, as seen by Baxendale and Wilson (15) and in earlier studies (4) by the present investigator. This parameter was measured for t-butanol using the simpler hydrogen peroxide photolysis system, as described in Section 4.

The starting point for modeling oxidant photolysis was the expression

$$P_a = \phi F I_o = \phi(1-10^{-\varepsilon c_a \bar{l}})I_o \quad , \tag{14}$$

adapted from Tournier and Deglise (38), where ϕ is the quantum yield (molecules reacted per photon absorbed), F is the fraction of incident photons absorbed, and I_o the incident photon intensity in Einsteins/(liter-unit time). The quantity F was to be evaluated from a Beers law-type expression where $\bar{l}$ is a parameter which serves as an "effective path length". The rigorous determination of F is quite a difficult problem, whereas the expression shown in equation 14 is a useful empirical relationship with some fundamental basis, using $\bar{l}$, the "effective path length", as a characteristic parameter of the particular photochemical reactor. Experimental verification of this expression is discussed in Section 4.

SECTION 4

RESULTS AND DISCUSSION

DEFINITION OF SYMBOLS

Upper Case

D = dose of an oxidant applied to the reactor

A = accumulated concentration of a specie in the reactor

R = reacted concentration of a substrate compound

P = photolyzed amount of an oxidant

I = UV intensity (Einsteins/L·min)

Lower Case Subscripts

o = ozone

h = hydrogen peroxide

a = applied dose (applies only to ozone)

u = utilized dose (applies only to ozone)

Using combinations of the above symbols, D_u is the utilized ozone dose, i.e. the amount of ozone which was removed from the gas stream, P_h was the amount of hydrogen peroxide photolysis, etc. The uppercase symbols may also represent rates, i.e. the dose rate, rate of accumulation, etc. It will be stated in the text whether the rate formalism or the integrated (cumulative) form is being used. It should be noted that the symbol I always represents a rate.

The experiments were divided into sets, according to the primary substrate: methanol, t-butanol, formaldehyde, formic acid, etc., and whether the process used was ozone/UV, ozone/H_2O_2, or H_2O_2/UV. These sets are shown in Table 2. Subsets of the sets shown in Table 2 corresponded to buffered, unbuffered, differing pH values, different feed gas flow rates, etc. Although runs were made at several different pH values, only the runs at pH 4.3 are discussed in this section. The reason for this limitation is that if a methanol or t-butanol reaction mixture is unbuffered its pH tends toward 4.3 ± 0.3 because of the organic acids which are produced. Thus, reactions begun at pH 4.3 tend to stay at

relatively constant pH. As will be seen below, the presence of buffers strongly affects the chemistry of the system. Unbuffered runs begun at other pH values changed pH during the run making mechanistic determination much more difficult. In addition, the base-catalyzed ozone decomposition (31) could be neglected at this pH.

Figure 5 shows the results of a typical ozone/UV experiment using methanol as the substrate, i.e. a set I experiment. Ozone flow to the reactor was begun at time t = 0. If lamps were used, they were already warmed up and stabilized, as was the ozone generator, prior to gas flow to the reactor. Methanol disappearance begins in Figure 5 after a short induction period, and ozone and/or peroxide begins to accumulate in the reactor. Early in the run, methanol is the major organic species in the reactor and mass balance relationship, such as given in Section 3, should hold. Use of early data is a common practice in kinetic studies to avoid the complexities introduced by products which occur later in the reaction. Similar experiments were run using different UV intensities and ozone dose rates to identify optimum reaction conditions. As described below, efficiency expressions developed in Section 3 (equations 10 and 11) were evaluated in terms of the measured parameters on the one hand, as well as in terms of available information on the efficiency of various steps (α, b, γ, δ, etc.). Thus, the left- and right-hand sides of equations 10 and 11 can be loosely regarded as "experimental" and "theoretical" sides. Agreement between the right-hand and left-hand side of equations 10 and 11, written in the rate form, was used to distinguish between Case I and Case II by evaluating the appropriate expression for ε_d. Before this could be done, however, it was necessary to determine at least reasonable ranges for some of the parameters in the model.

Measurement of Hydrogen Peroxide Photolysis Rate

One rate which is required but not directly measurable during an ozone/UV experiment was the peroxide photolysis rate, P_h. Aqueous solutions of hydrogen peroxide were photolyzed in the CSTPR in order to model peroxide photolysis according to equation 14. Several different peroxide

concentrations were used with four different lamp intensity combinations: 0, 1, 2, and 3-1/2 lamps. Peroxide concentration versus time was plotted to obtain the rate of peroxide disappearance, which was then fit to

$$\text{Rate} = K_1(1 - 10^{-K_2 C}) \qquad (15)$$

where C is the peroxide concentration. The value of K_2 which gave the best fit to all the data was determined to be 149.4 M^{-1}. The best K_1 was then determined for each lamp intensity. These values are given in Table 3. Linear regression of these values gave a small non-zero intercept which corresponded closely to the experimentally measured dark reaction rate and a slope of 0.483×10^{-4} M min^{-1}. Identification of K_2 in equation 15 with $\varepsilon\bar{l}$ in equation gave an effective path length $\bar{l}$ of 7.6 cm, using ε = 19.6 M^{-1} cm^{-1} from Baxendale and Wilson (15). Similarly, $\phi I_o = K_1$ so that with ϕ = 1 (0.5 for the primary process x 2 hydroxyl radicals produced) and ignoring the dark rate, the intensity of one lamp was found to be 8.5 L (4.8×10^{-5} E/L-min) = 4.08×10^{-4} E/min = 3.2 W.

The data is shown in Figure 6 as discrete points while the solid lines are the curve fit using the above parameters. Agreement with experiment is seen to be good except at $[H_2O_2] = 10^{-1}$ M and lower intensities where higher rates are observed, and for two lamps below $[H_2O_2] = 3 \times 10^{-4}$. These results confirmed the usefulness of applying equation 14 for describing photochemical reactions and for characterizing photochemical reactors using the effective path length $\bar{l}$. They also provided a means of estimating the peroxide photolysis rate, P_h, in the mathematical analysis of O_3/UV data.

Hydrogen Peroxide Photolysis in the Presence of t-Butanol

Because of the simplicity of the system, H_2O_2 photolysis experiments with oxygen sparging were used to obtain values of δ for empirical use in the evaluation of mass balance expressions for the t-butanol data. The reaction system is as follows:

$$H_2O_2 \xrightarrow{h\nu} 2 \cdot OH \quad (16)$$

$$OH + CH_3(CH_3)_2COH \longrightarrow \cdot CH_2(CH_3)_2COH + H_2O \quad (17)$$

$$O_2 + \cdot CH_2(CH_3)_2COH \longrightarrow \underset{(I)}{O_2CH_2(CH_3)_2COH} \quad (18)$$

$$2\ I \longrightarrow H_2O_2 + \text{other products} \quad (19)$$

This gives rise to the flow diagram and mass balance relationships shown in Figure 7. Since the products of t-Butanol (t-BuOH) destruction are not known, it is necessary to evaluate the parameters from data taken early in the reaction, in order to avoid complications introduced by the presence of products. The parameter β is then the efficiency of t-BuOH destruction by $\cdot OH$, or the fraction of $\cdot OH$ produced which successfully attacks t-BuOH. The calculated value of γ which results is thus an instantaneous efficiency (γ at a particular time, t) rather than an average over the run (i.e. $\gamma_{ave} = t^{-1}\int_0^t \gamma\ dt$). These calculations lead to a value of $\gamma \cong 0.70$. Since it is not known how γ varies with reaction conditions, a range of γ about the calculated value was used in the further calculations which follow.

Computer Model of Methanol Systems

A few methanol experiments were run in which all stable products (i.e. methanol, formic acid and formaldehyde) were determined. Typical experimental results for the analytes are shown in Figure 8. The pH of the solution during the run is shown in Figure 9. The pH variation in this experiment is much greater than in experiments where methanol and t-butanol were the major species initially present. It was desirable to model the concentration profiles of the stable products 1) to gain confidence in our model of the mechanistic pathway, 2) to test the suitability of literature rate constants in such a calculation, and 3) to alleviate the need to measure all reaction products during an experimental run. This last point could increase greatly the number of experiments which could be performed in a given time. A computer simulation was used to model experimental results for the system

$$\text{Methanol} \xrightarrow{\cdot OH} \text{Formaldehyde} \xrightarrow{\cdot OH} \text{Formic Acid} \qquad (20)$$

The program, used the differential mass balance equations

$$\frac{d[M]}{dt} = K_1[M][H] \qquad (21)$$

$$\frac{d[F]}{dt} = K_1[M][H] - K_2[F][H] \qquad (22)$$

$$\frac{d[FA]}{dt} = K_2[F][H] - K_3[FA][H] - K_4[FA][O] \qquad (23)$$

where: M = methanol concentration
H = hydroxyl radical concentration
F = formaldehyde concentration
FA = formic acid + formate concentration
O = ozone concentration

For simplicity, Euler's Method (39), with a time increment of 1/200 of the total run time, was used to step through the reaction series. Literature values (40,41) of the second order rate constants were used and K_3 and K_4 were broken up into the sum of rate constants for formic acid and formate times their respective fractions at that pH. To estimate the hydroxyl radical concentration, equation 21 was solved at regular intervals using experimental data and literature rate constants.

The reaction of formate and formic acid directly with ozone was included in the model; however, for evaluation of R_T (discussed below) it was assumed to be negligible since these species accounted for less than 6% of the total substrate concentration.

The simulation predicted the total substrate concentration at any time during the run (Figure 10) with an error of less than 9%. Thus, with the computer model an estimation of the relative substrate concentrations can be obtained by monitoring only the methanol concentration. Rate constants from the literature were seen to model this reaction system quite suitably.

Evidence Supporting the Proposed Mechanism

By rearranging the mass balance equations derived from Figures 3 and 4, a parameter, ε_d, may be defined to be a function of theoretical efficiencies and also as a function of measurable experimental quantities. The two candidate mechanisms give different forms of ε_d, shown earlier in equations 10 and 11.

$$\varepsilon_d{}^{I} \equiv \frac{R_T}{D_u - A_o - A_H + P_H\,(3/\alpha - 1)} = \frac{2}{(3/\alpha\beta - \gamma - (1 - \gamma)\delta)} \qquad (10)$$

and for mechanism II

$$\varepsilon_d{}^{II} \equiv \frac{R_T}{D_u - A_o + A_H\,(2 - \alpha) + P_H\,(3 - \alpha)} = \frac{2}{[1/\beta + (2 - \alpha)(\gamma + (1 - \gamma)\delta)} \qquad (11)$$

Before the parameter ε_d may be calculated for either mechanism the efficiency α must be evaluated. From rate constant data the values of β and γ were determined to be approximately 1.0 for the methanol system. Using this approximation, α may be solved for directly by rearranging equations 10 and 11. For mechanism I the value of α follows a smooth curve throughout the run, and ranges from 0.87 to 0.51 (Figure 11). Calculated values for mechanism II were, in most cases, negative, having an average of -0.24 and a standard deviation of 0.54. A negative value of alpha has no physical significance, so that subsequent data was evaluated for case II using a range of values of α which is more reasonable in light of the reaction sequence. Put another way, for the same reaction solution conditions there is no reason to expect α to vary widely with substrate identity.

The failure of α to be well-behaved for case II is, however, already an indication of the inappropriateness of that reaction scheme. It remains to be demonstrated that case I is appropriate. Values of the parameter ε_d were calculated for both mechanisms using experimental data, values of alpha, β, and γ derived as explained above, and the following expressions:

$$\varepsilon_d{}^{I}{}_P \equiv \frac{R_P}{Du - A_O - A_H + P_H\,(3/\alpha - 1)} = \frac{2}{\left[(3/\alpha\beta + \eta(1 - 1/\beta) - \gamma - \delta(1 - \gamma)\right]} \qquad (28)$$

$$\varepsilon_d{}^{II}{}_P \equiv \frac{R_p}{D_u - A_O + A_H\,(2 - \alpha) + P_H\,(3 - \alpha)} =$$

$$\frac{2}{\left[1/\beta + (2 - \alpha)\,[\gamma + (1 - \gamma)\delta + (1/\beta - 1)\eta\right]} \qquad (29)$$

where subscript P indicates parent compound value. These expressions were derived exactly as were equations 10 and 11, but R_P refers only to parent compound. This was necessary because it was desirable to analyze t-butanol data using the same expression. Since no product data is available for t-butanol, R_T cannot be calculated as it was for methanol. Thus, an additional pathway with efficiency $(1 - \beta)\eta$ must be added to include active species feedback in the form of superoxide produced by reaction of hydroxyl radical with products other than parent compound. For these expressions to be valid in this application, β must refer only to parent compound. The approximation for β given in equation 13 was used.

Measurable properties and efficiencies have been separated to the greatest extent possible in equations 28 and 29, so that the left-hand side represents a sort of "experimental" quantity while the right-hand side can be considered a "theoretical" value. The "theoretical" and "experimental" values of εd_p for the two mechanisms were calculated for laboratory data for both tertiary butanol and methanol, and are summarized in Table 4. The results indicate that mechanism I is the more accurate representation of the laboratory data, with all but one experimental $\varepsilon_d{}^{I}{}_P$ being within the mechanistically predicted range. Experimental values of $\varepsilon_d{}^{I}$ fall towards the lower end of the theoretical range indicating that the initial values of 1.0 assumed for β and γ when calculating alpha are probably not quite correct and should be slightly less. Theoretical values of ε_d given by mechanism II are about 1.5 to 6 times the experimentally obtained results.

Oxidation Efficiency

Ozone Utilization Efficiency. By measuring the methanol concentration and using the computer simulation to estimate the concentrations of formaldehyde, formic acid, and formate for an experiment, an evaluation of the ozone utilization efficiency, $(R_T/D_u)_c$, can be made. R_T is here defined as the molar concentration of organic substrate that has reacted with hydroxyl radical. For example, one mole of methanol reacts to make one mole of formaldehyde, which makes one mole of formic acid/formate which in turn forms one mole of carbon dioxide. When all organic substrate has oxidized, in this example, R_T would be three moles. The utilized ozone dose rate, D_u, is then numerically integrated to give the cumulative utilized ozone dose. Thus $(R_T/D_u)_c$ is the efficiency with which substrate molecules are destroyed by ozone, on a mole-to-mole basis. This efficiency can be evaluated at any degree of conversion of parent compound by evaluating the total amount of organic species remaining at that point, and integrating D_u from t = 0 to the corresponding time.

For methanol, the pH-buffered systems give the ratio $(R_T/D_u)_c$ of approximately 1 on a molar basis as the normalized parent substrate concentration, C/Co, approaches zero as shown in Figure 12a. However, for unbuffered methanol solutions, $(R_T/D_u)_c$ as a function of C/Co has the form shown in Figure 12b and increases to a value greater than unity in some cases. As a function of the number of UV lamps, $(R_T/D_u)_c$ evaluated at C/Co = 0.5 shows the relationship given in Figure 13. For unbuffered solutions (R_T/D_{uc}) is a smooth curve which appears to have a minimum, then increases as the number of UV lamps is increased. The pH buffered solution shows a maximum utilized ozone efficiency at about one lamp.

An examination of mechanism I (Figure 3) shows that photolysis of ozone produces hydrogen peroxide, some of which in turn can be photolyzed to produce two hydroxyl radicals. As the number of UV lamps is increased, the maximum efficiency $(R_T/D_u)_c$ would theoretically approach 2.0. Mechanism II predicts that 2 hydroxyl radicals are produced directly from the photolysis of an ozone molecule, giving the same limiting $(R_T/D_u)_c$ as mechanism I.

By examining Figure 14, a comparison of ozone concentrations in aqueous solution for buffered and unbuffered systems shows a higher ozone concentration for buffered systems when greater than three-quarters of a lamp was used. This is caused by a decrease in the demand for ozone by the reaction series (Figure 3) but is not currently well understood.

In Figure 15 the maximum hydrogen peroxide concentration as a function of the number of UV lamps is shown. The hydrogen peroxide concentrations in the buffered solutions are markedly lower even though, according to Beer's Law, ozone should photolyze to hydrogen peroxide (mechanism I) at an equal or faster rate than is seen in the unbuffered system. This indicates that side reactions of hydrogen peroxide and/or hydroxyl radical are present in buffered solution. Two reactions which are known (42,18) to occur are

$$H_2PO_4^- + \cdot OH \rightarrow \cdot HPO_4^- + H_2O \qquad (24)$$

and

$$\cdot HPO_4^- + H_2O_2 \rightarrow H_2PO_4^- + HO_2\cdot \qquad (25)$$

In addition, phosphate radical ion (HPO_4^-) reacts with organic compounds, with typical second-order rate constants in the range of $10^7 - 10^8$ M^{-1} s^{-1} (18) compared to $k_{23} = 2.2 \times 10^6$ (42) and $k_{24} = 2.7 \times 10^7$ (18). Thus, a significant portion of phosphate radical ion may react with organic compound with no great effect on β. However, consumption of phosphate radicals by equation 25 would be expected to lower the overall efficiency of the process. Thus, the point in Figure 13 at which the efficiency falls off in buffered solutions may be the point at which so much ozone is photolyzed that not enough is left to react with superoxide which is produced by equation 25 followed by dissociation of HO_2:

$$HO_2 \rightleftharpoons H^+ + O_2^- \qquad (26)$$

So far a consistent interpretation of the data for phosphate buffered systems shown in Figures 12-14 has not been found. Research is underway (42) to better understand the important effect which added solutes may have on the efficiency of free radical processes.

Capture Efficiency. Consideration of the destruction efficiency based on the utilized ozone dose (R_T/D_u) is useful for mechanistic considerations; however, the amount of ozone utilized by the reaction and the amount applied to the reactor are not the same. The ratio of the utilized ozone dose (that removed from the gas stream) to the applied ozone dose (total ozone bubbled through the reactor), D_u/D_a, is a measure of the percentage of ozone "captured" by the reaction system and is thus called the capture efficiency. Both the buffered and unbuffered systems show an increase in the capture efficiency as the number of UV lamps is increased (Figure 16). A comparison of the capture efficiency for the two types of solutions shows that unbuffered solutions have a higher ozone reaction rate when more than 3/4 of a lamp is used. Since ozone photolysis, reaction with formic acid/formate, and reaction with superoxide are the major ozone-consuming reactions in this system, it is clear that the presence of the buffer causes definite enhancement/inhibition effects on one or more of these reactions. Both curves extrapolate to very low values of D_u/D_a, indicating that the solutions would absorb very little ozone in the absence of UV irradiation.

As would be expected from a mass transfer viewpoint, an increase in the impeller speed to 750 rpm was seen to increase the capture efficiency; however, as the ozone feed flow rate increases, the capture efficiency decreases. This is probably because an increase in the ozone mass transfer attributable to increased gas-liquid contact area is offset by a shorter contact time, so that a gas "flooding" condition exists, coupled with the fact that the system appears to be reaction rate-limited.

Applied Ozone Efficiency. From an economic perspective, the applied ozone efficiency, $(R_T/D_a)_c$, is an important parameter. It is the total amount of substrate disappearance divided by the applied ozone dose. While no attempt was made during the mechanistic study to operate under

optimum conditions for mass transfer, the identification of factors which are important in determining optimum conditions is an important part of this study.

The $(R_T/D_a)_c$ curves for both systems, Figure 17, resemble the $(R_T/D_u)_c$ curves in Figure 12. For a buffered system it would be desirable to operate at the maximum $(R_T/D_a)_c$ to achieve the most organic oxidation for the amount of ozone input to the reactor. For an unbuffered system a detailed economic analysis would be required to determine the optimum operating conditions, since at very high UV intensities the system approaches the H_2O_2/UV system. Both buffered and unbuffered systems should theoretically approach the limiting value of 2.0 as the number of lamps is increased.

Characteristic Substrate Reduction Time

The time, $\tau(n)$, required to reduce substrate concentration to e^{-n} times its initial value is defined as the characteristic substrate reduction time. In a practical sense this parameter is related to reactor sizing and thus to capital cost for a treatment process. For a first order reaction

$$C/C_o = e^{-kt} \qquad (27)$$

so that at $C/C_o = e^{-1}$, $t = \tau(1) = k^{-1}$. For reactions which are not first order, τ has less fundamental significance but is still of interest. In unbuffered systems this time decreased smoothly as the number of UV lamps was increased (Figure 18). However, for buffered systems the characteristic time shows a minimum. This would be expected from examination of the curves of R_T/D_u (Figure 12) and R_T/D_a (Figure 17) for buffered solutions, and can be explained by the reduction of ozone utilization efficiency due to side reactions as mentioned in previous sections.

SECTION 5

SUMMARY AND CONCLUSIONS

It has been demonstrated that the mechanistic model depicted in Figure 3 is useful for describing the complex photolytic ozonation reaction system. In this model, ozone participates mainly in three reactions:

1. Direct reaction with organic solutes
2. Photochemical conversion to hydrogen peroxide
3. Reaction with superoxide generated in solution by secondary reactions

Hydroxyl radicals are produced by the reaction 3 as well as from photolysis of the hydrogen peroxide produced by reaction 2. These hydroxyl radicals react with organic compound to produce organic radicals which in turn react quickly with oxygen to produce organic peroxy radicals. These peroxy radicals cause feedback of active species into a cyclic reaction system either by decomposing to yield superoxide and a stable organic molecule, or by reacting through complicated reactions to yield hydrogen peroxide. Superoxide then "activates" incoming ozone through reaction 3 above.

The strength of this reaction system as a treatment process results from two characteristics:

1) The hydroxyl radical formed can convert virtually any organic compound to carbon dioxide and water.
2) The reaction system is extremely versatile in that there are several reaction pathways which can be followed, depending on solution conditions.

As an example of 2 above, if superoxide is not formed from the compounds which are present in solution, hydrogen peroxide will accumulate until its photolysis produces enough hydroxyl radical for the reaction to proceed. As smaller molecules are produced, superoxide production will resume. Figure 3 shows that there are at least three different reactions which produce hydroxyl radical and at least two reactions which give active

species feedback to the cycle after organic compound is attacked. Because of this versatility, the O_3/UV and H_2O_2/UV systems are not equivalent, even though ozone photolysis produced hydrogen peroxide.

It can be seen from this study that "autodecomposition" of ozone in solution can only aid organic removal. Despite early publications (43) which pointed out this fact, there still exists a widespread misconception that "decomposed ozone is lost ozone".

The photochemical reaction model presented in equation 14 was shown to describe hydrogen peroxide photolysis adequately, allowing prediction of the reaction rate from knowledge of peroxide concentration in solution, the quantum yield of the reaction, and the number of lamps being used. It remains to calculate ozone photolysis rates from the mechanistic model and, by comparison with the photochemical reactor model, determine whether ozone photolysis rates are predictable by this same model. This cannot be done directly as it was for peroxide because side reactions cannot be eliminated experimentally without causing other chain reactions.

Most importantly, the mechanistic model can be used to determine optimum conditions for photolytic ozonation, based on cumulative destruction efficiencies, discussed in Section 4. The data from the conditions giving the highest value of $(R_T/D_u)_c$ can be analyzed using the model to determine which parts of the reaction sequence were of most importance. In many cases the trade-off between reaction efficiency (which for a treatment process translates directly into ozone generating capability) and speed of reaction (reactor size, number of stages, etc.) will require interfacing of the mechanistic model with an economic analysis of the process. It was seen that solute effects such as those introduced by the presence of a pH buffer in the laboratory or perhaps naturally present in ground water can strongly alter the chemistry and efficiency of the process. More study is needed in order to understand these solute effects in the complicated ozone/UV system.

Finally, means need to be developed to extend these concepts to more complicated molecules and mixtures. Toward this end, a better understanding of the degradation pathways of organic molecules in hydroxyl radical systems is needed.

Future Work

The effect of added solutes on the efficiency of hydroxyl radical reactions is currently under study in this laboratory (42), as is the application of the mechanistic model to two more complex organic molecules, diethyl malonate and diethyl phthalate (44). Assembly of a Mobile Oxidation Pilot Plant (MOPP) is scheduled to begin soon in order to evaluate photolytic ozonation and the concepts developed during the present study on "real-world" waters at the field scale.

Acknowledgements

The authors would like to acknowledge financial support of the Water Resources Center at the University of Illinois, Urbana, for this project, as well as that of the Illinois State Water Survey for salary support for the principal investigator. We are also grateful to Mr. J. Keith Carswell and USEPA Water Engineering Research Laboratory, Drinking Water Research Division, Cincinnati, Ohio, for the loan of ozone generating and monitoring equipment.

REFERENCES

1. Glaze, W. H., G. R. Peyton, F. Y. Huang, J. L. Burleson, and P. C. Jones. Oxidation of Water Supply Refractory Species by Ozone with Ultraviolet Radiation, Final Report, EPA-600/2-80-110, August, 1980.

2. Peyton, G. R., F. Y. Huang, J. L. Burleson, and W. H. Glaze. "Destruction of Pollutants in Water with Ozone in Combination with Ultraviolet Radiation, 1. General Principles and Oxidation of Tetrachloroethylene." Environ. Sci. Technol. 16 (1982): 448.

3. Glaze, W. H., G. R. Peyton, S. Lin, F. Y. Huang, and J. L. Burleson. "Destruction of Pollutants in Water with Ozone in Combination with Ultraviolet Radiation, 2. Natural Trihalomethane Precursors." Environ. Sci. Technol. 16 (1982): 454.

4. Glaze, W. H., G. R. Peyton, B. Sohm, and D. A. Meldrum. "Pilot Scale Evaluation of Photolytic Ozonation for Trihalomethane Precursor Removal." Final Report to USEPA/DWRD/MERL, Cincinnati, OH, Cooperative Agreement #CR-808825, J. Keith Carswell, Project Officer, 1984.

5. Garrison, R. L., C. E. Mauk, and H. W. Prengle, Jr. "Advanced Ozone-Oxidation System for Complexed Cyanides." 1st International Symposium on Ozone for Water and Wastewater Treatment. Edited by R. G. Rice, and M. E. Browning, International Ozone Institute, Syracuse, N.Y., 1975.

6. Prengle, H. W., Jr., C. G. Hewes III, and C. E. Mauk. In Proceedings of 2nd International Symposium on Ozone Technology, p. 211. Edited by R. G. Rice, P. Richet, and M. A. Vincent, International Ozone Institute, Syracuse, NY, 1975.

7. Prengle, H. W., Jr., C. E. Mauk, and J. E. Payne. "Ozone/UV Oxidation of Chlorinated Compounds in Water." Presented at the International Ozone Institute Forum on Ozone Disinfection, Chicago, Illinois, June 2-4, 1976.

8. Prengle, H. W., Jr. and C. E. Mauk. "Ozone/UV Oxidation of Pesticides in Aqueous Solution." In Ozone/Chlorine Dioxide Oxidation Products of Organic Materials, edited by R. G. Rice and J. A. Cotruvo. (1978): 302. Ozone Press International, Cleveland, Ohio.

9. Fochtman, E. G. and J. E. Huff. "Ozone-Ultraviolet Light Treatment of TNT Wastewaters." In Proceedings of 2nd International symposium on Ozone Technology, p. 211. Edited by R. G. Rice, P. Richet, and M. A. Vincent, International Ozone Institute, Syracuse, N.Y., (1975).

10. McCarthy, J. J., W. F. Cowen, and E. S. K. Chian. "Evaluation of an Air Stripping-Ozone Contactor System." In Proceedings of the 32nd Industrial Waste Conference, pp. 310-324. Purdue University, 1977.

11. Leitis, E., E. H. Bryan, J. D. Zeff, D. C. Crosby, and M. Smith. "An Investigation into the Chemistry of the UV/Ozone Purification Process." Presented at the 4th World Ozone Congress, Houston, Texas, November 27-29, 1979.

12. Kuo, P. P. K., E. S. K. Chian, and B. J. Chang. "Identification of End Products Resulting from Ozonation and Chlorination of Organic Compounds Commonly Found in Water." Environmental Science and Technology 11 (1977): 1177.

13. Taube, H. Transactions of the Faraday Society 53 (1957): 656.

14. Taube, H. and W. C. Bray. J. Am. Chem. Soc. 62 (1940): 3357.

15. Baxendale, J. H. and J. A. Wilson. Transactions of the Faraday Society 53 (1957): 344.

16. Peyton, G. R. and W. H. Glaze. "The Mechanism of Photolytic Ozonation." In Proceedings of the Symposium on Aquatic Photochemistry." 189th Annual Meeting of the American Chemical Society, April, 1985. In press as an ACS monograph entitled "Aquatic Photochemistry."

17. Peyton, G. R. and W. H. Glaze. "Photolytic Ozonation: A Mechanistic Perspective." Ozonews 13 (1985): #4.

18. Ross, A. B. and P. Neta. Rate Constants for Reactions of Inorganic Radicals in Aqueous Solution, NSRDS-NBS 65, p. 5, 1979.

19. Horak, J. and J. Pasek. Design of Industrial Chemical Reactors from Laboratory Data, p. 358. Heyden & Son, Inc., Philadelphia, 1978.

20. Prengle, H. W., Jr. III, C. G. Hewes, and C. E. Mauk. In Proceedings of 2nd International Symposium on Ozone Technology, p. 224. Edited by R. G. Rice, P. Richet and M. A. Vincent, International Ozone Institute, Syracuse, N.Y., 1975.

21. Bader, H. and J. Hoigne. Water Res. 15 (1981): 449.

22. Bader, H. and J. Hoigne. Ozone: Science and Engineering 4 (1982): 169.

23. Flamm, D. L.. Environ. Sci. Technol. 11 (1977): 978.

24. Hart, E., K. Sehested, and J. Holcman. Anal. Chem. 55 (1983): 46.

25. Parker, G. A. Colorimetric Determination of Nonmetals, p. 301. Edited by D. R. Boltz and J. A. Howell, Wiley, 1928.

26. Masschelein, W. J., M. Davis, and R. Ledent. Water and Sewage Works, August 1977, p. 69.

27. Houle, M. J., D. E. Long, and D. Smette. Anal. Lett. 3 (1970): 401-409.

28. Bethge, P. O. and K. Lindstrom. Analyst 99 (1974): 137-42.

29. Parker, C. A.. In Proceedings of the Royal Society A, 220 (1953): 104.

30. Sauer, M. C., Jr.; W. G. Brown; and E. J. Hart. "O(^{3}P) Atom Formation by the Photolysis of Hydrogen Peroxide in Alkaline Aqueous Solutions." J. Phys. Chem. 88 (1984): 1398-1400

31. Staehelin, J. and J. Hoigne. "Decomposition of Ozone in Water: Rate of Initiation by Hydroxide Ions and Hydrogen Peroxide." Environ. Sci. Technol. 16 (1982): 676.

32. Buhler, R. F., J. Staehelin, and J. Hoigne. J. Phys. Chem. 88 (1984): 2560.

33. Rabani, J., D. Klug-Roth, and A. Henglein. J. Phys. Chem. 78 (1974): 1089-2093.

34. Willson, R. L. Trans. Faraday Soc. 67 (1971): 3008.

35. Swallow, A. J. Prog. Reaction Kinetics 9 (1978): 195-366.

36. Bielski, B. H. J., D. E. Cabelli, R. L. Arudi, and A. B. Ross. J. Phys. Chem. Ref. Data 14 (1985): 1041-1100.

37. Moore, J. W. and R. G. Pearson. Kinetics and Mechanism. Wiley, N.Y., 1981.

38. Tournier, A. and X. Deglise. J. Photochem. 18 (1982): 47.

39. Reiss, E. L., A. J. Callegari, D. S. Ahluwalia. Ordinary Differential Equations with Applications. Holt, Rinehart and Winston, Chicago, Illinois, 1976.

40. Hoigne, J. and H. Bader. "Rate Constants of Reactions of Ozone with Organic and Inorganic Compounds in Water-I." Water Research 17 (1983): 173-183.

41. Farhataziz and A. B. Ross. Selected Specific Rates of Reactions of Transients From Water in Aqueous Solution. III. Hydroxyl Radical and Perhydroxyl Radical and Their Radical Ions, NSRDS-NBS 59, January 1977 (available from NTIS).

42. Peyton, G. R. "Solute Effects in Aquifer Cleanup/Hazardous Waste Treatment by Oxy-Radical Processes." Project currently underway for the Hazardous Waste Research and Information Center, Champaign, Illinois. Scheduled completion date, August 31, 1987.

43. Hewes, C. G., and R. R. Davidson. AIChE J. 17 (1971): 141-147.

44. Peyton, G. R. "Laboratory Scale Investigation of Ozone/UV Treatment of Leachate and Chemical Agent Simulants." Project underway for U. S. Army Construction Engineering Research Laboratory, Champaign, Illinois. Scheduled completion date, Sept. 30, 1987.

45. Sehested, K., J. Holeman, and E. J. Hart, J. Phys. Chem. 87 (1983): 1951-54.

46. Christensen, H., K. Sehested, and H. Corfitzan, J. Phys. Chem. 86 (1982): 1588.

TABLE 1

SELECTED BIMOLECULAR RATE CONSTANTS FOR THE POP SYSTEM[a]

	H_2O_2	HO_2^-	HO_2	O_2^-	OH	O_2
O_3	<0.2(14)	2.8×10^6(31)	$<10^4$(45)	1.6×10^9(32)	1.1×10^8(45)	NR
H_2O_2	NR	NR	3.7(36)	0.2^{-3}(36)	2.7×10^7(46)	NR
HO_2^-		NR	NR(b)	<2(36)	7.5×10^9(41)	NR
HO_2			8.3×10^5(36)	9.7×10^7(36)	7.1×10^9(36)	NR
O_2^-				<0.3(36)	1.0×10^{10}(36)	NR
OH					4×10^9(41)	NR
HCO_3^-	--	--	--	$1\text{-}2 \times 10^6$(36)	1.5×10^7(31)	NR
$\cdot HCO_3$				$1\text{-}4 \times 10^8$(36)	--	NR
CH_3OH				--	9×10^8(41)	--
$\cdot CH_2OH$				--	--	4.2×10^9(33)
CH_2O				--	6.9×10^8(41)	--
HCO_2H				--	1.5×10^8	--
HCO_2^-				<0.01(36)	3.5×10^9(41)	--
$\cdot CO_2^-$				--	(c)	2.4×10^9(36)

NOTES:

a) All rate constants in $(mol/L)^{-1}sec^{-1}$. Numbers in parentheses following rate constants are reference numbers.

b) This reaction can be considered negligible, since $pK_{H_2O_2} = 11.6$ while $pK_{HO_2} = 4.8$.

c) Not found but undoubtedly fast, i.e. 10^9-10^{10}.

TABLE 2

EXPERIMENT SETS

Substrate	Treatment Process		
	O_3/UV	O_3/H_2O_2	H_2O_2/UV
Methanol	I	I_2	
t-butanol	II		II_3
formaldehyde	III		
formic acid	IV		

TABLE 3

EXPERIMENTALLY DETERMINED K_1 VALUES[a]

Number of lamps	$10^4 K_1$, M min^{-1}	$10^4 K_1$ from linear regression
0	0.05	0.051
1	0.547	0.534
2	0.999	1.018
3-1/2	1.75	1.74

NOTES:

a) See equation 15 and text for discussion

TABLE 4

EXPERIMENTAL VS. THEORETICAL EFFICIENCY[a]

Substrate	Buffer	c/c_o	E_d^I Theor.[c][g]	E_d^I Exp'T'L[b][f]	E_d^{II} Theor.[e][g]	E_d^{II} Exp.'T'L[d][f]
Methanol	None	0.8	0.51 ± 0.09	0.56 ± 0.03	0.35 ± 0.06	0.79 ± 0.06
		0.9	0.57[h]	0.56 ± 0.03	0.24[h]	0.79 ± 0.06
	0.01 M phosphate	0.8	0.54 ± 0.15	0.56 ± 0.03	0.50 ± 0.15	0.79 ± 0.06
		0.9	--	0.56 ± 0.03	--	0.79 ± 0.06
t-Butanol	None	0.8	0.41 ± 0.15	0.44 ± 0.07	0.37 ± 0.16	0.90 ± 0.09
		0.9	0.63[h]	0.49 ± 0.07	0.16[h]	1.01 ± 0.09
	0.01 M phosphate	0.8	0.37 ± 0.17	0.44 ± 0.07	0.29 ± 0.14	0.90 ± 0.09
		0.9	0.50 ± 0.10	0.49 ± 0.07	0.22 ± 0.08	1.01 ± 0.09

NOTES:

a) As defined by equations 28 and 29. Initial pH 4.3.
b) Left-hand side of equation
c) Right-hand side of equation
d) Left-hand side of equation
e) Right-hand side of equation
f) Deviation represents range of experimental values.
g) Deviation represents range of ε_d produced by the parameteric ranges listed in Table 5.
h) Single measurement

TABLE 5

VALUES OF PARAMETERS USED IN CALCULATION OF ε_d[a]

Parameter	Value	
	Methanol	t-butanol
α	0.82-0.87	0.7-0.9
β	c/c_o[b]	c/c_o[b]
γ	1	0
δ	0.7	0.7
η	0-1	0-1

NOTES

a) ε_d listed in Table 4
b) of parent compound

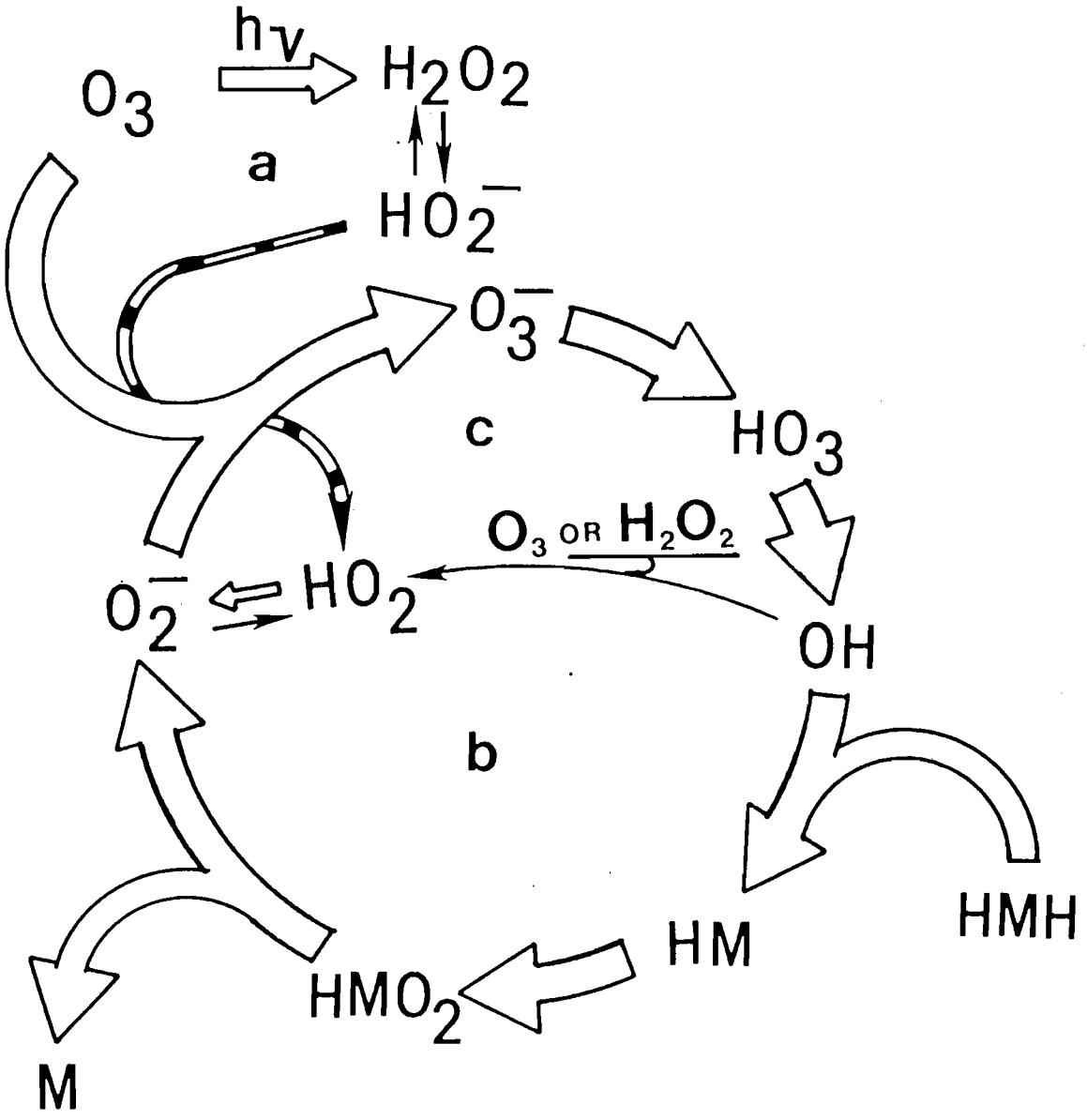

Figure 1. Prototype mechanism from Peyton and Glaze (17).

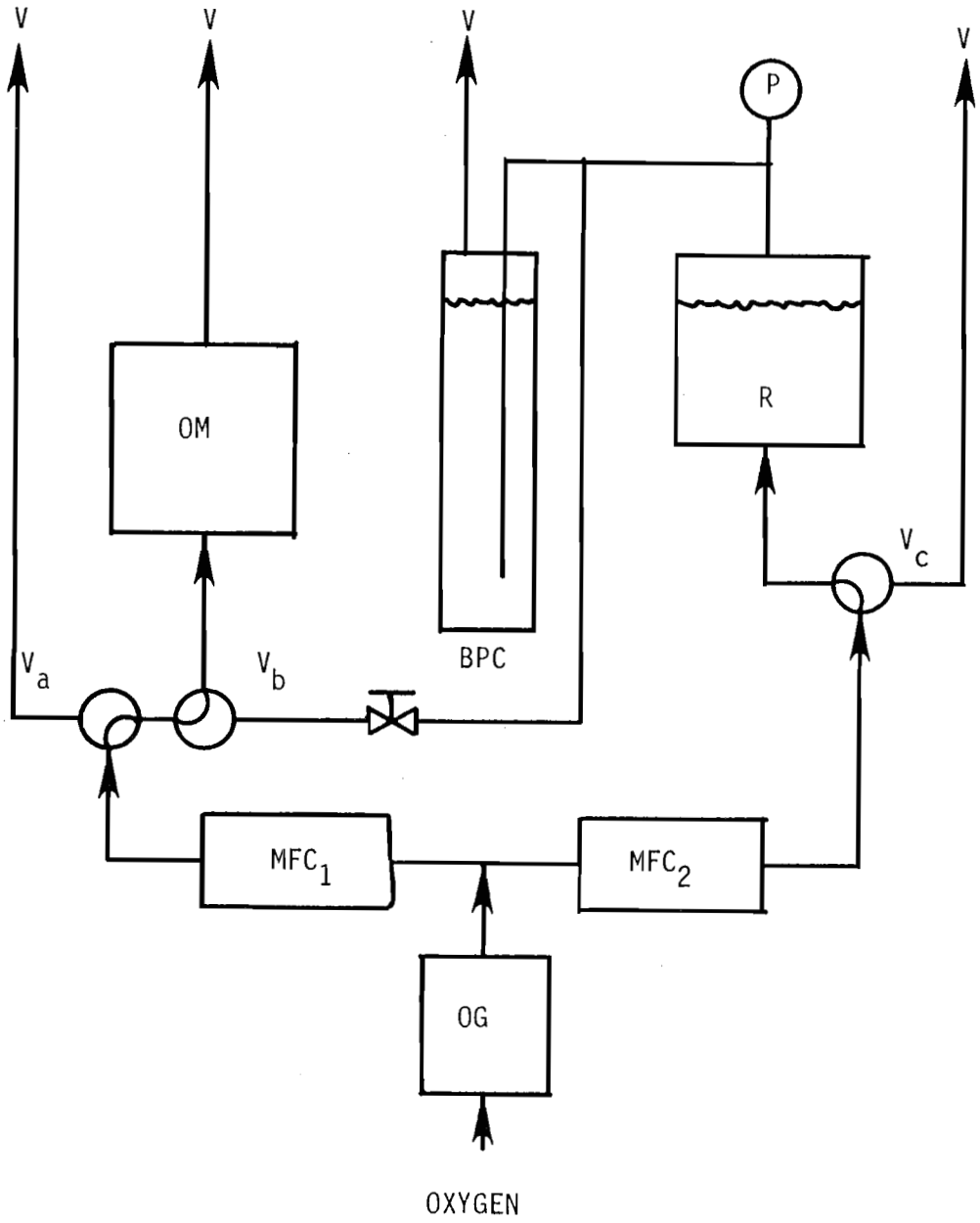

Figure 2. Experimental apparatus. Symbols explained in text.

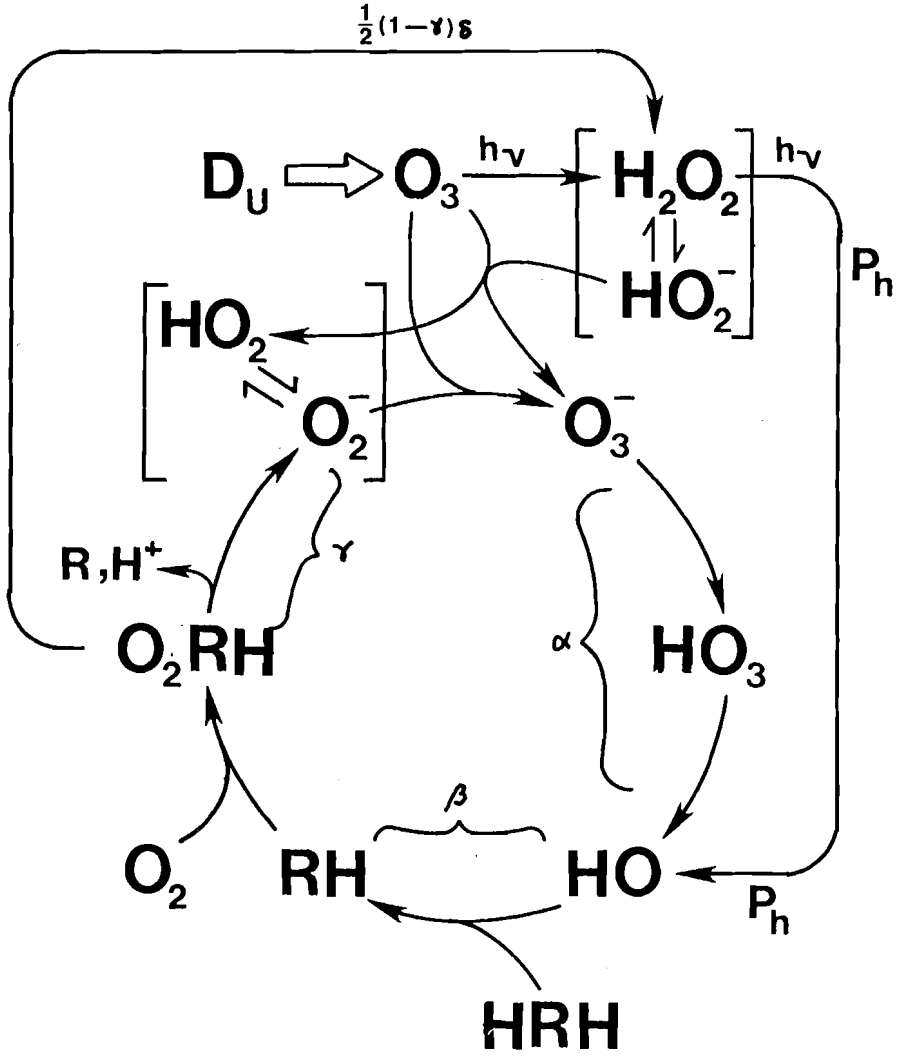

Figure 3. Scheme I.

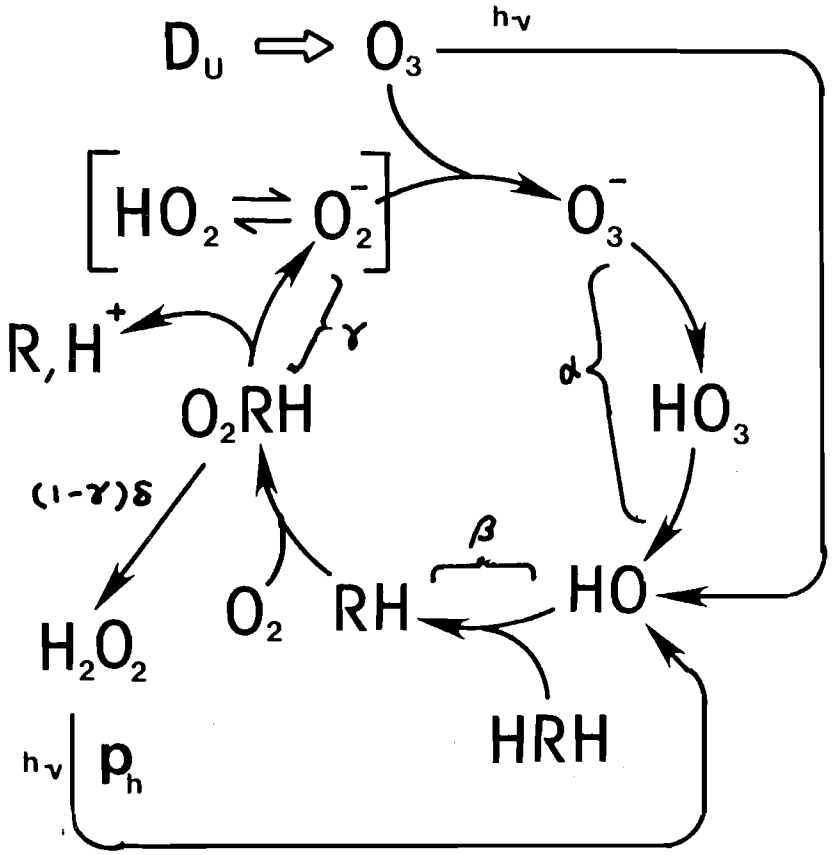

Figure 4. Scheme II.

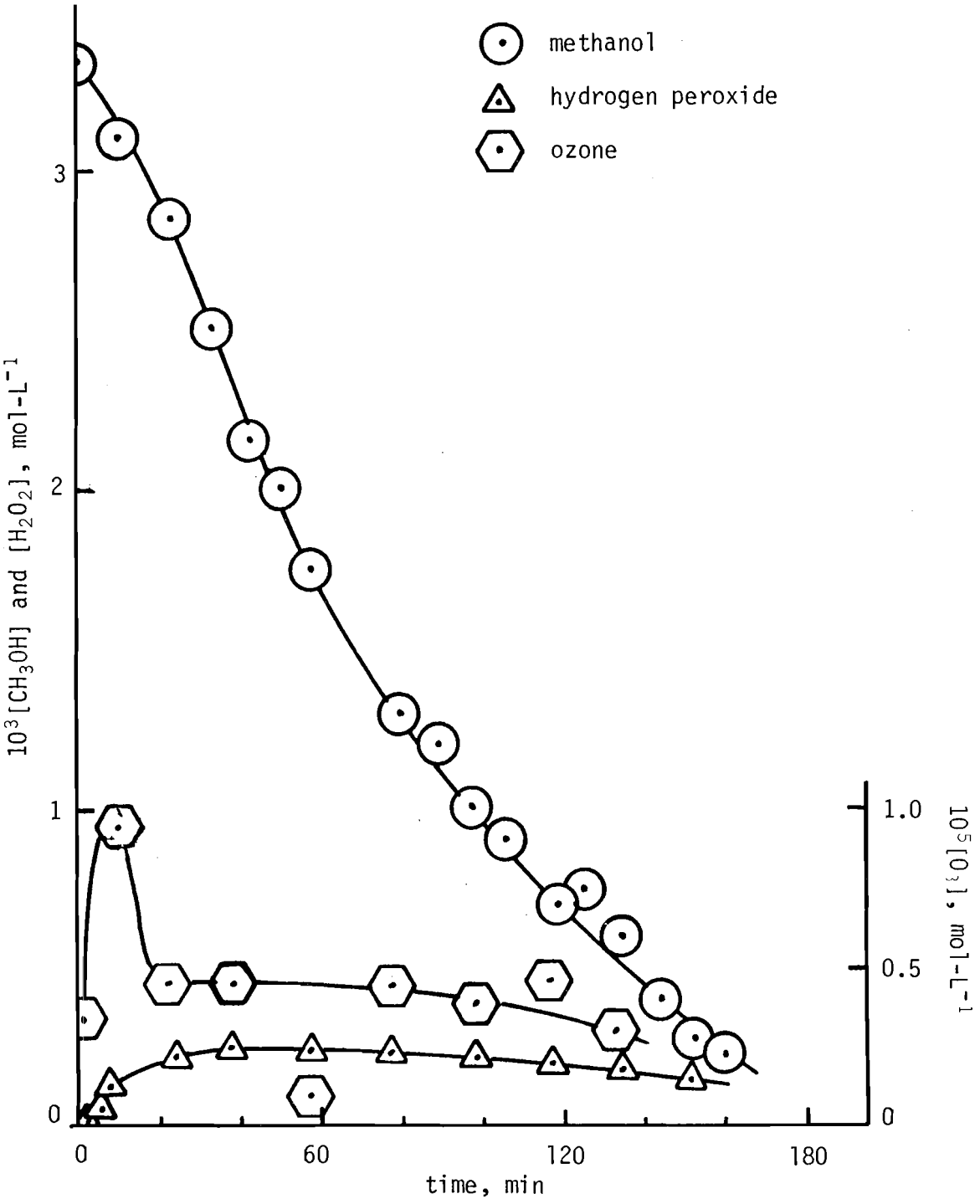

Figure 5. Data from a typical photolytic ozonation experiment.

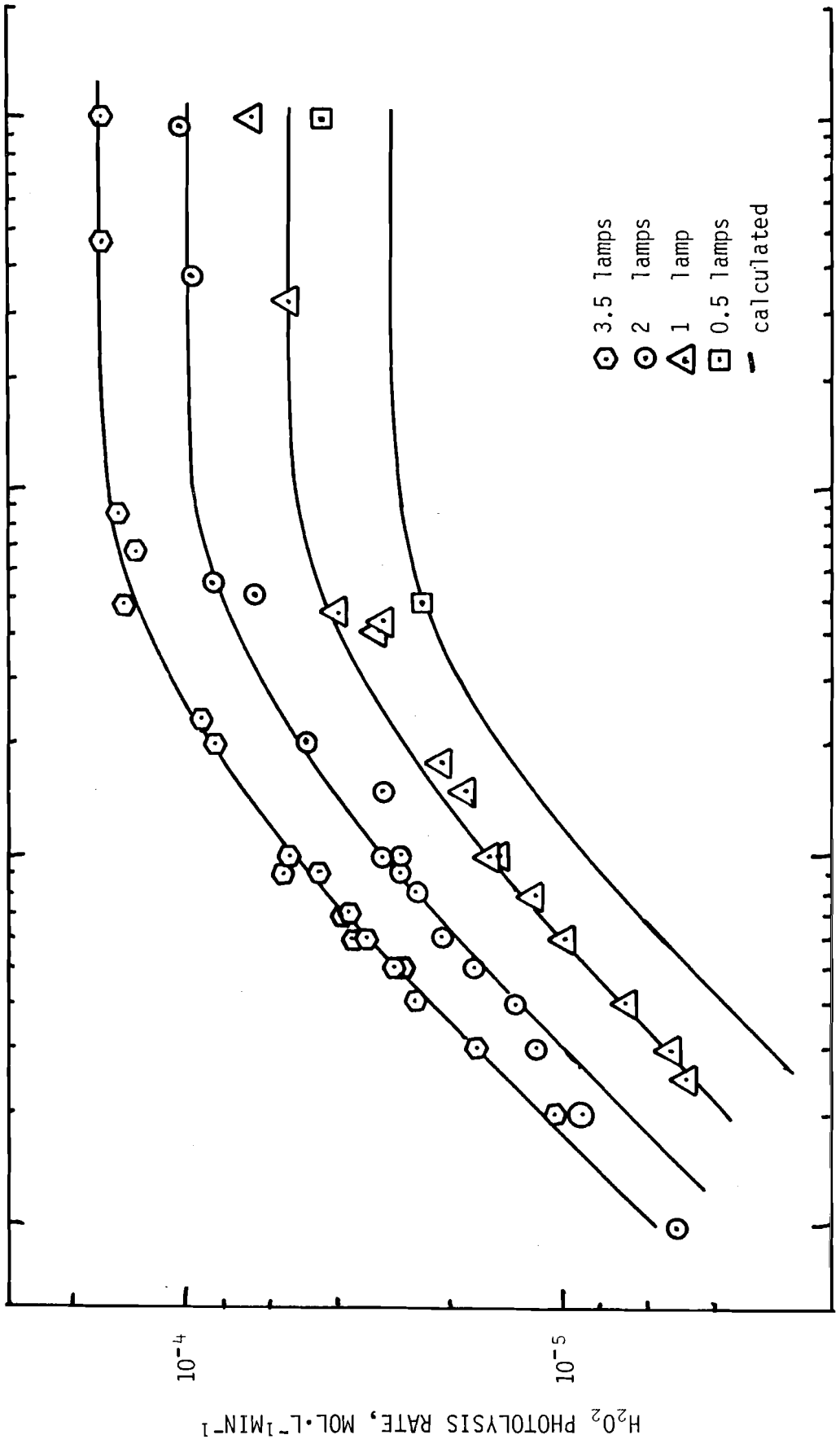

Figure 6. Modeling hydrogen peroxide photolysis rate in CSTPR.

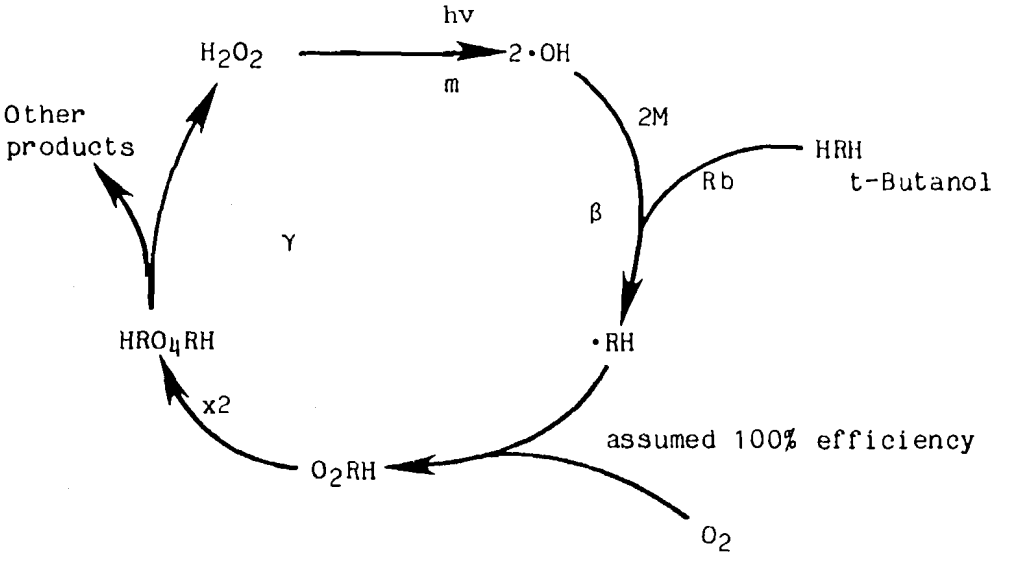

$$\gamma\beta m = A_H + M \quad (A_H < 0)$$
$$R_b = 2\beta M$$

assuming $\beta = 1$ leads to

$$\gamma = \frac{2A_H}{R_b} + 1$$

Figure 7. Flow diagram for hydrogen peroxide photolysis in the presence of t-butanol.

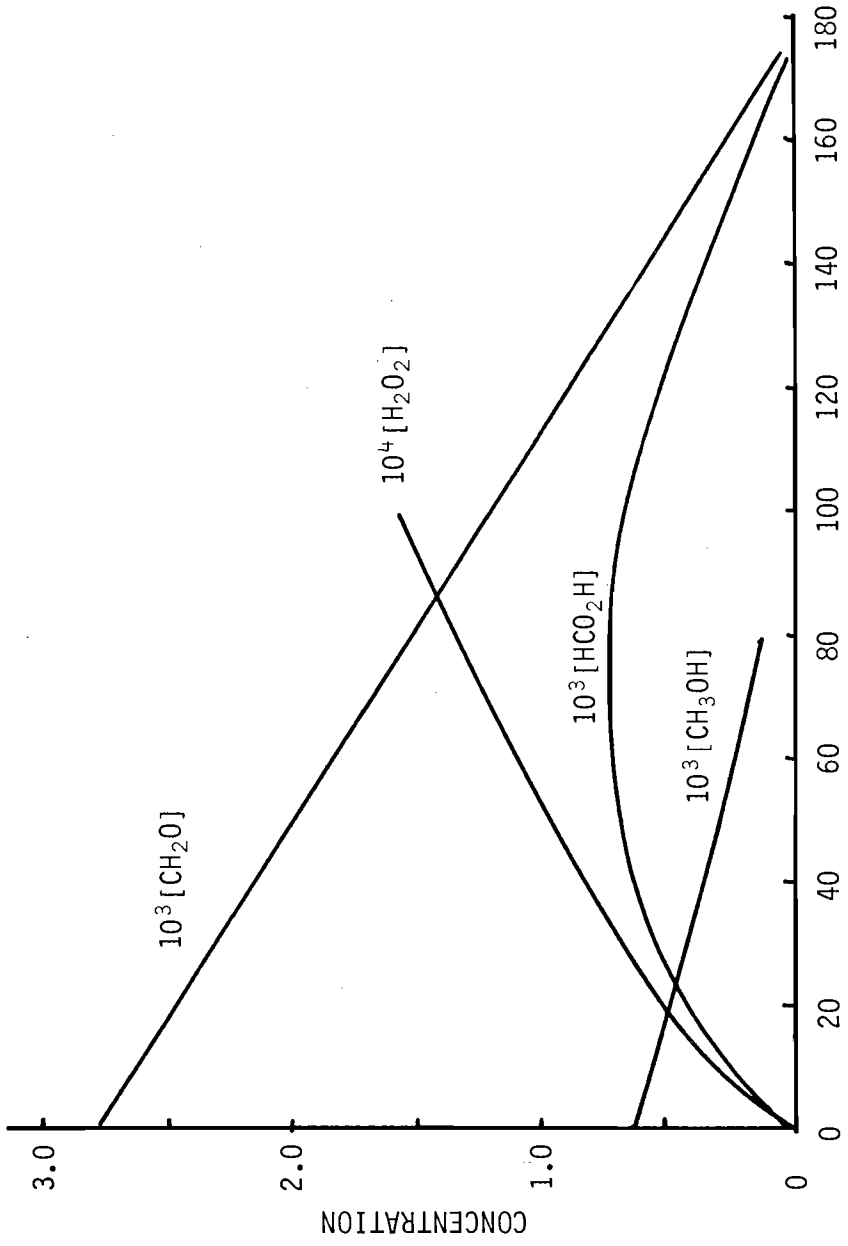

Figure 8. Reactant concentrations during model calibration run.

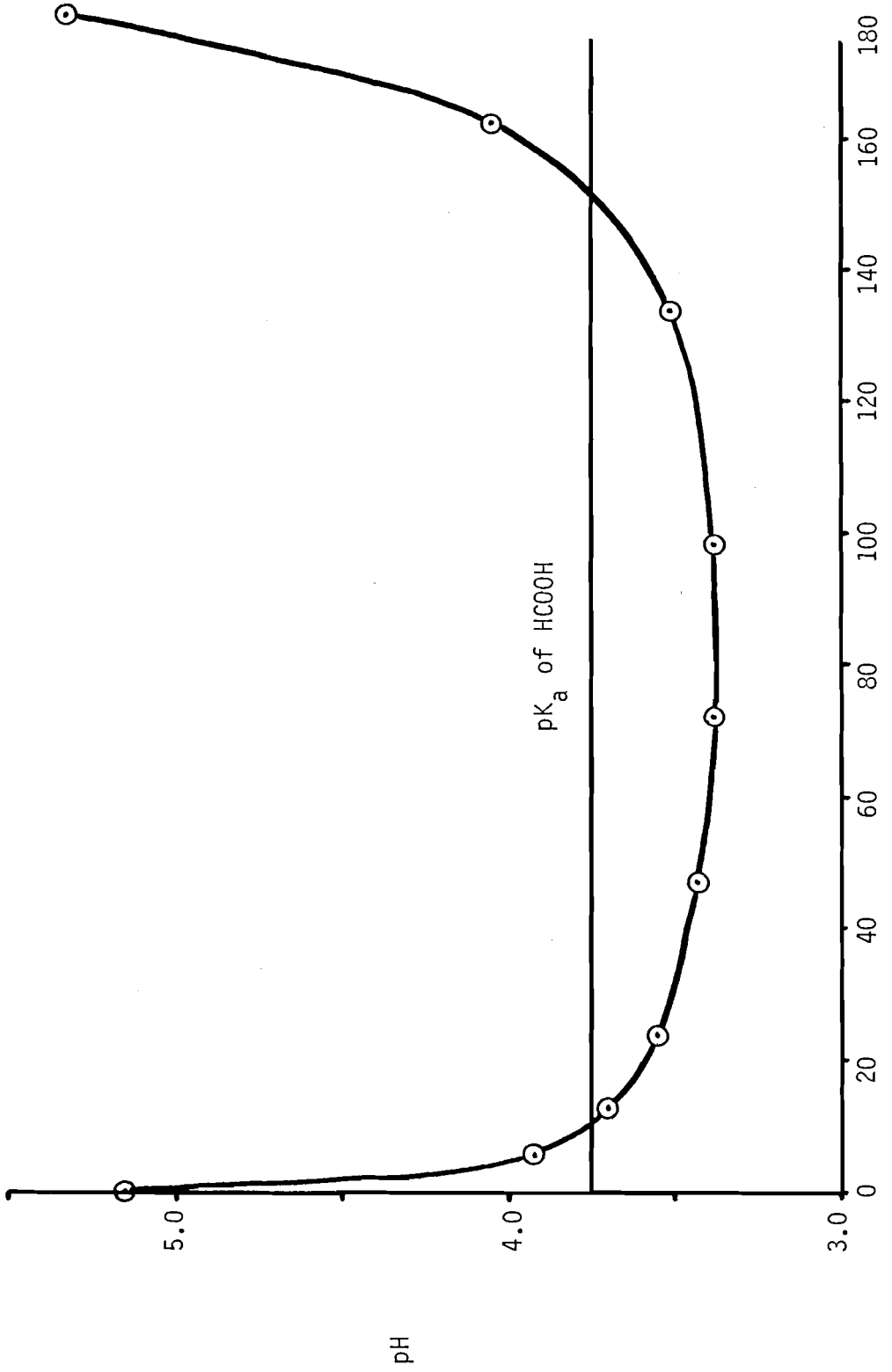

Figure 9. pH during model calibration run.

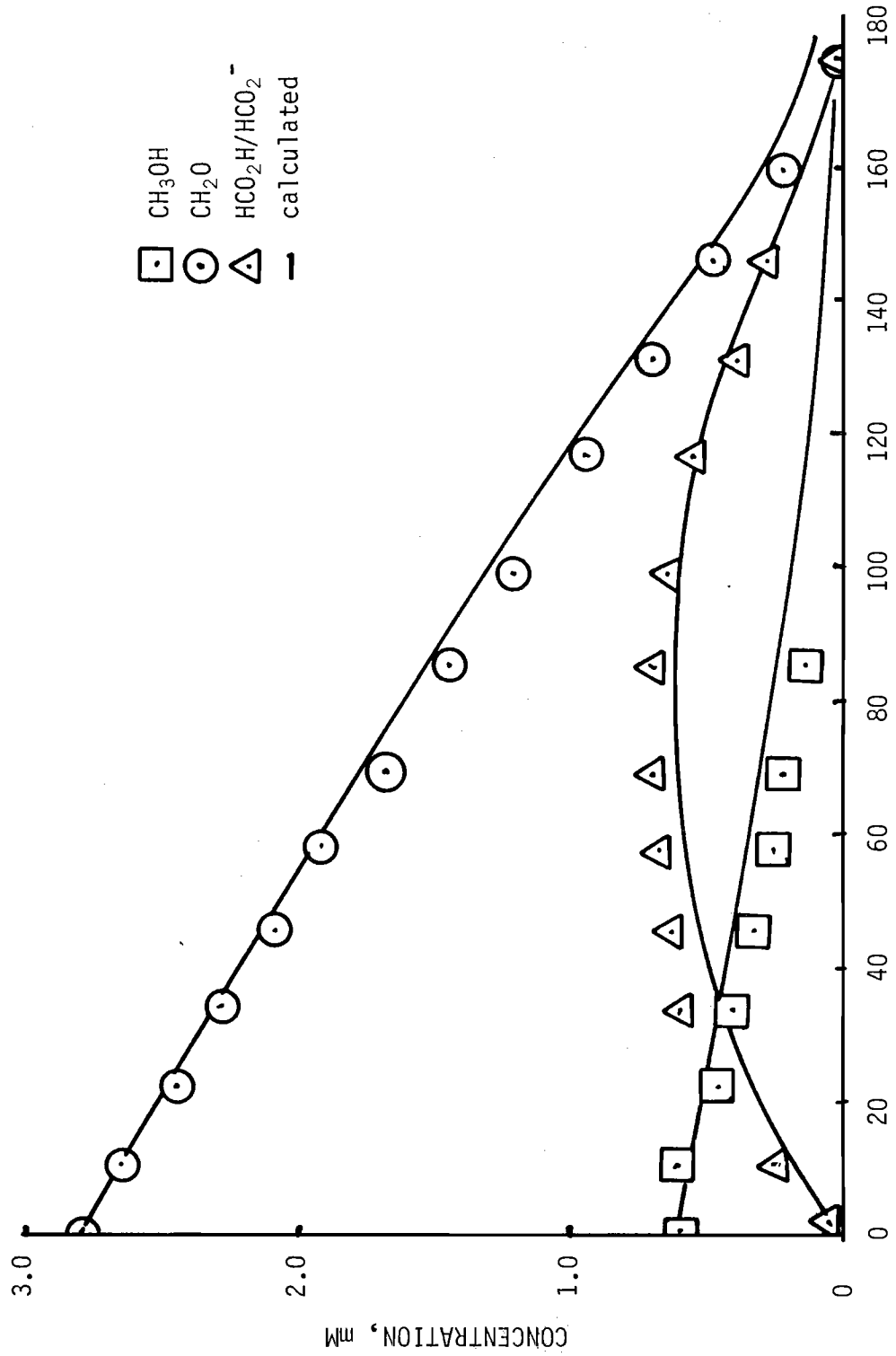

Figure 10. Fit of calibration run data using literature rate constants.

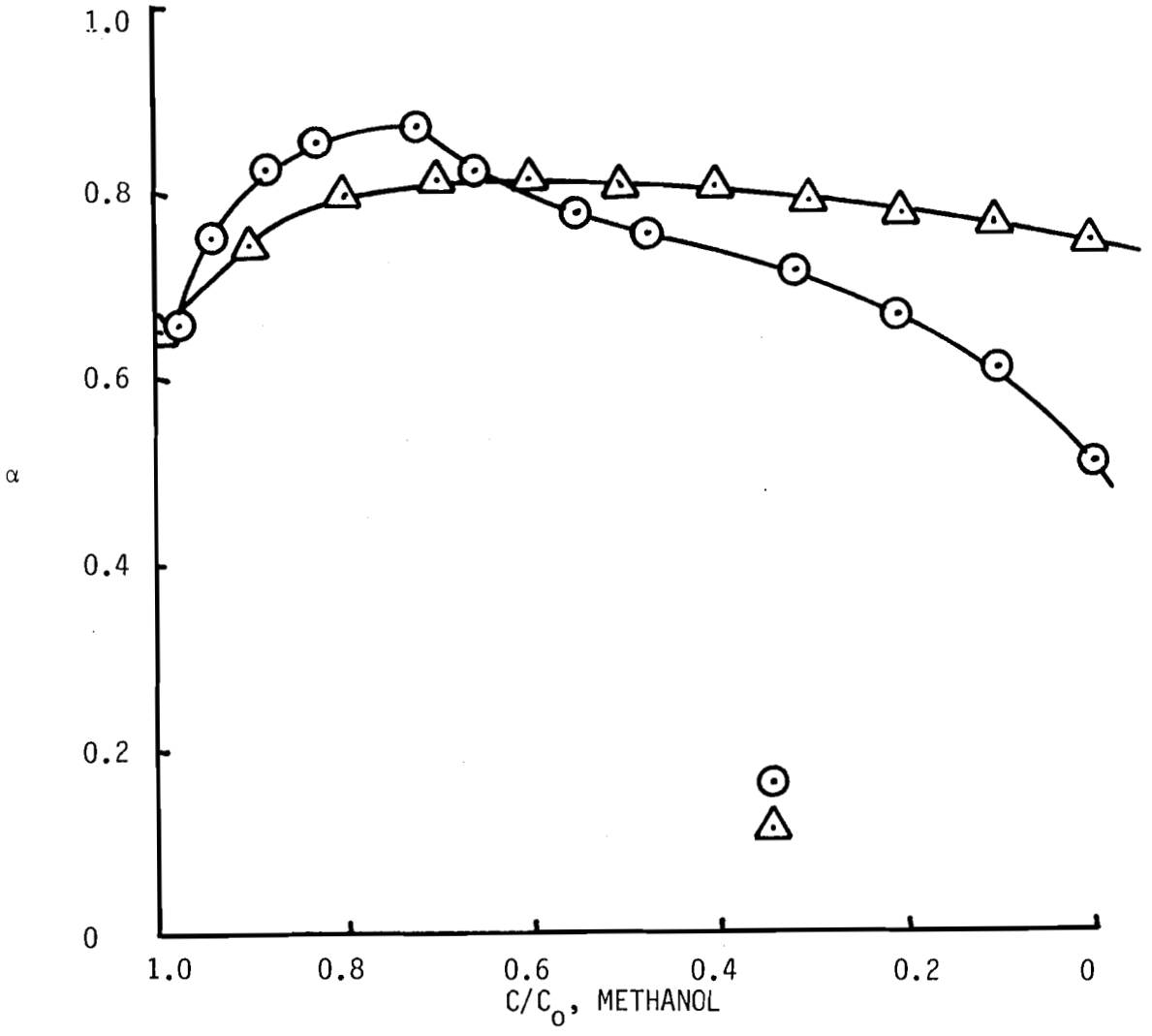

Figure 11. Variation of efficiency parameter, α, during the calibration run.

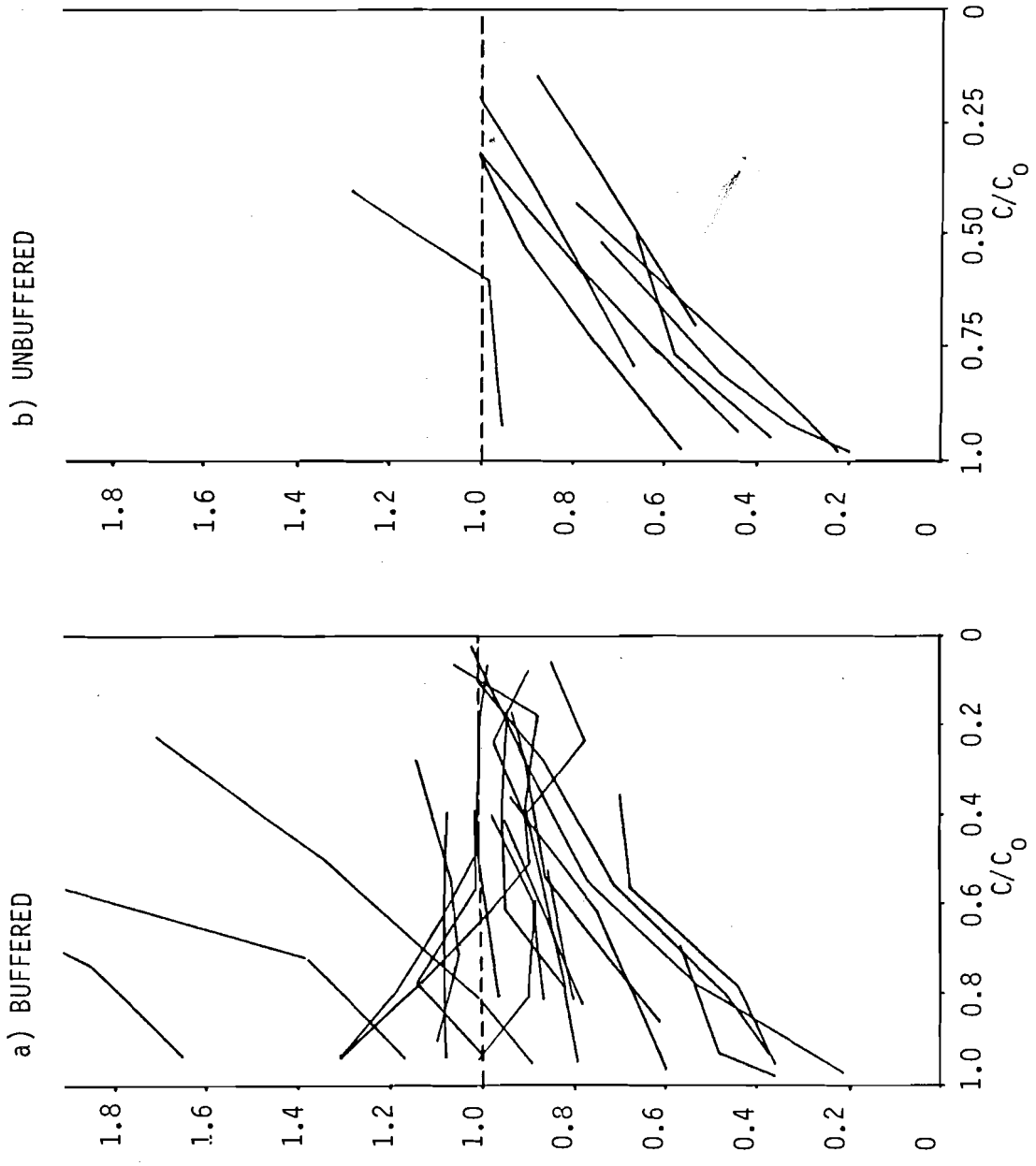

Figure 12. Ozone utilization efficiency in methanol experiments.

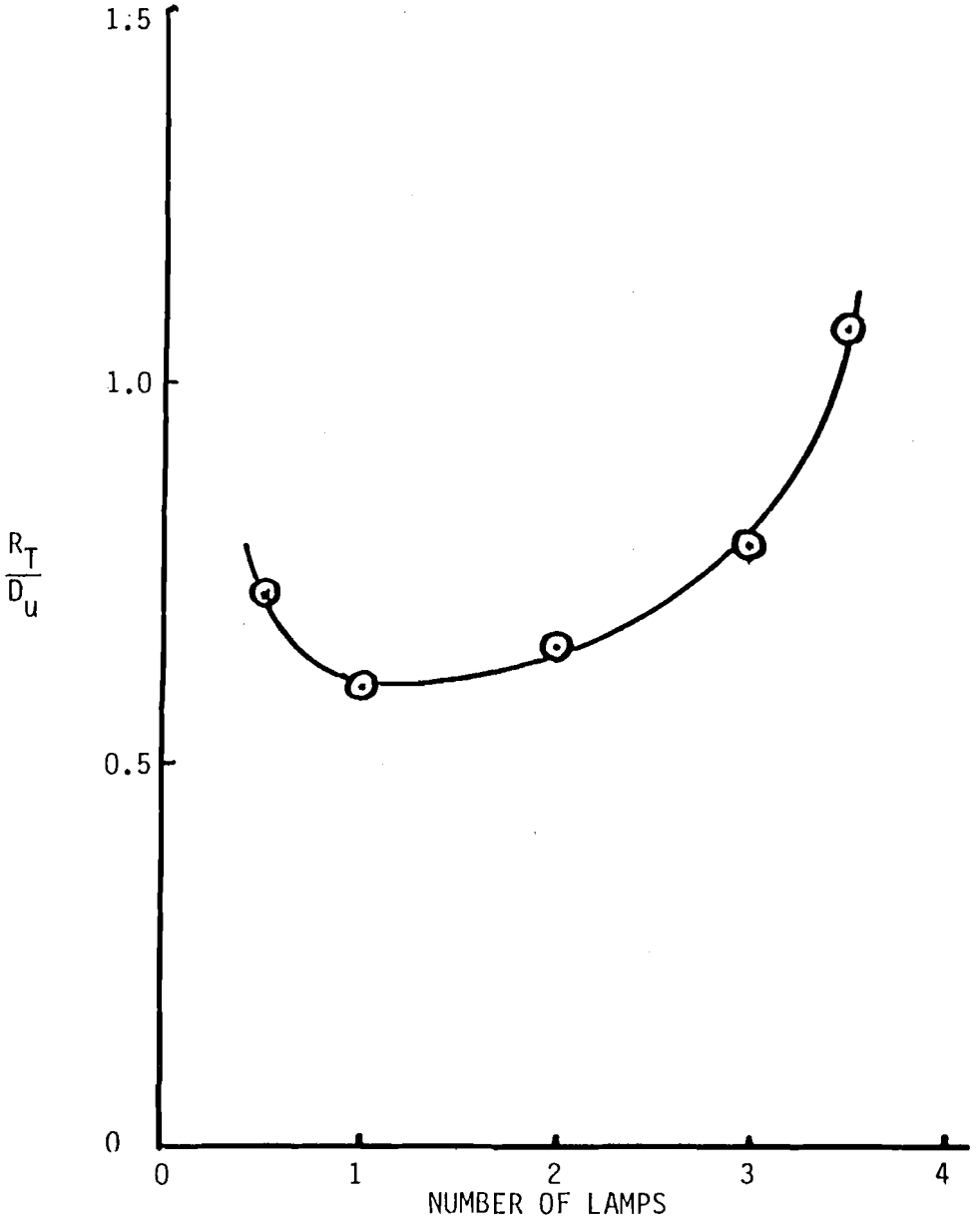

Figure 13. Ozone utilization efficiency at $C/C_0 = 0.5$ during methanol experiment. Symbols explained in text.

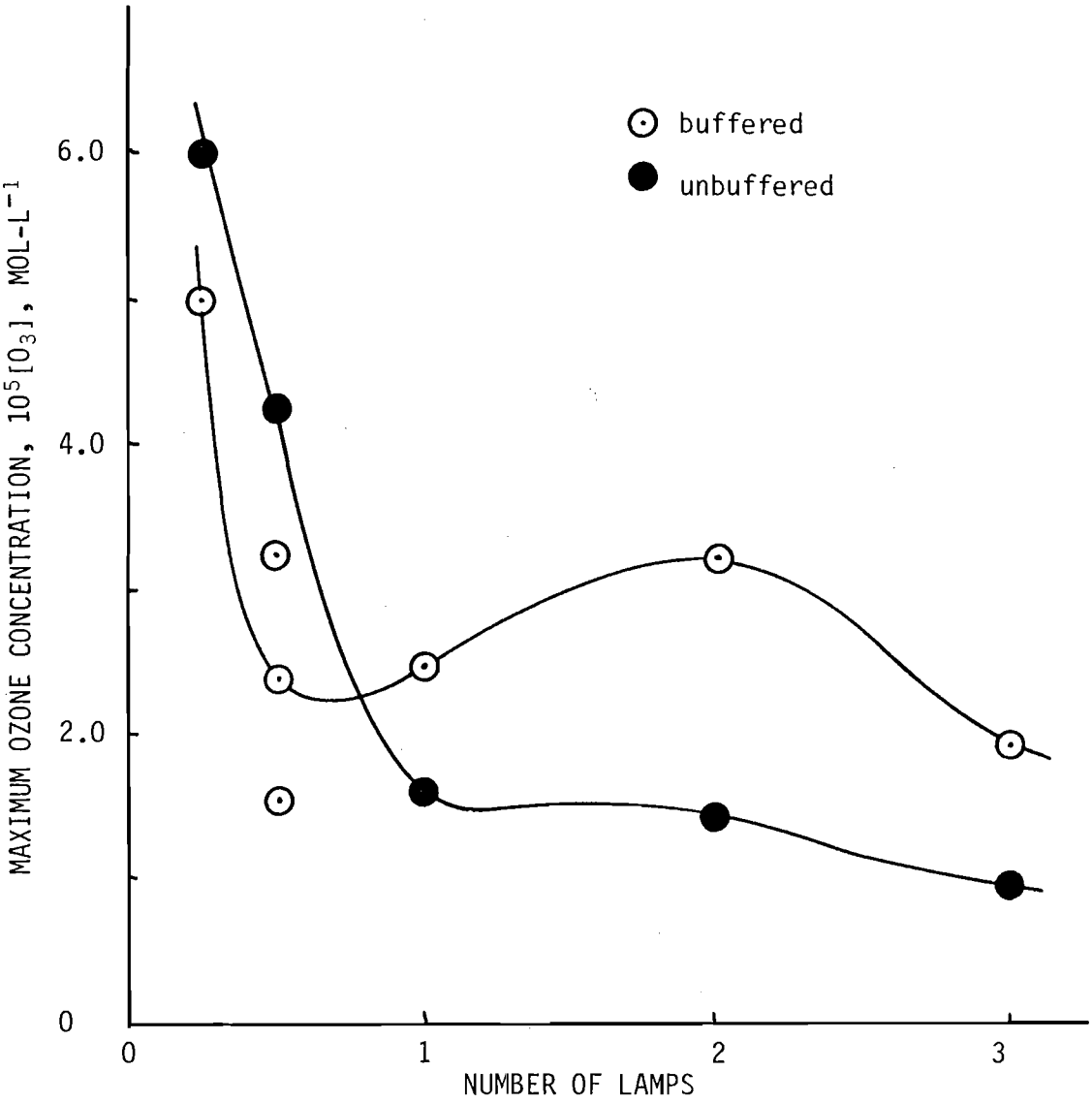

Figure 14. Maximum ozone concentration during methanol experiments.

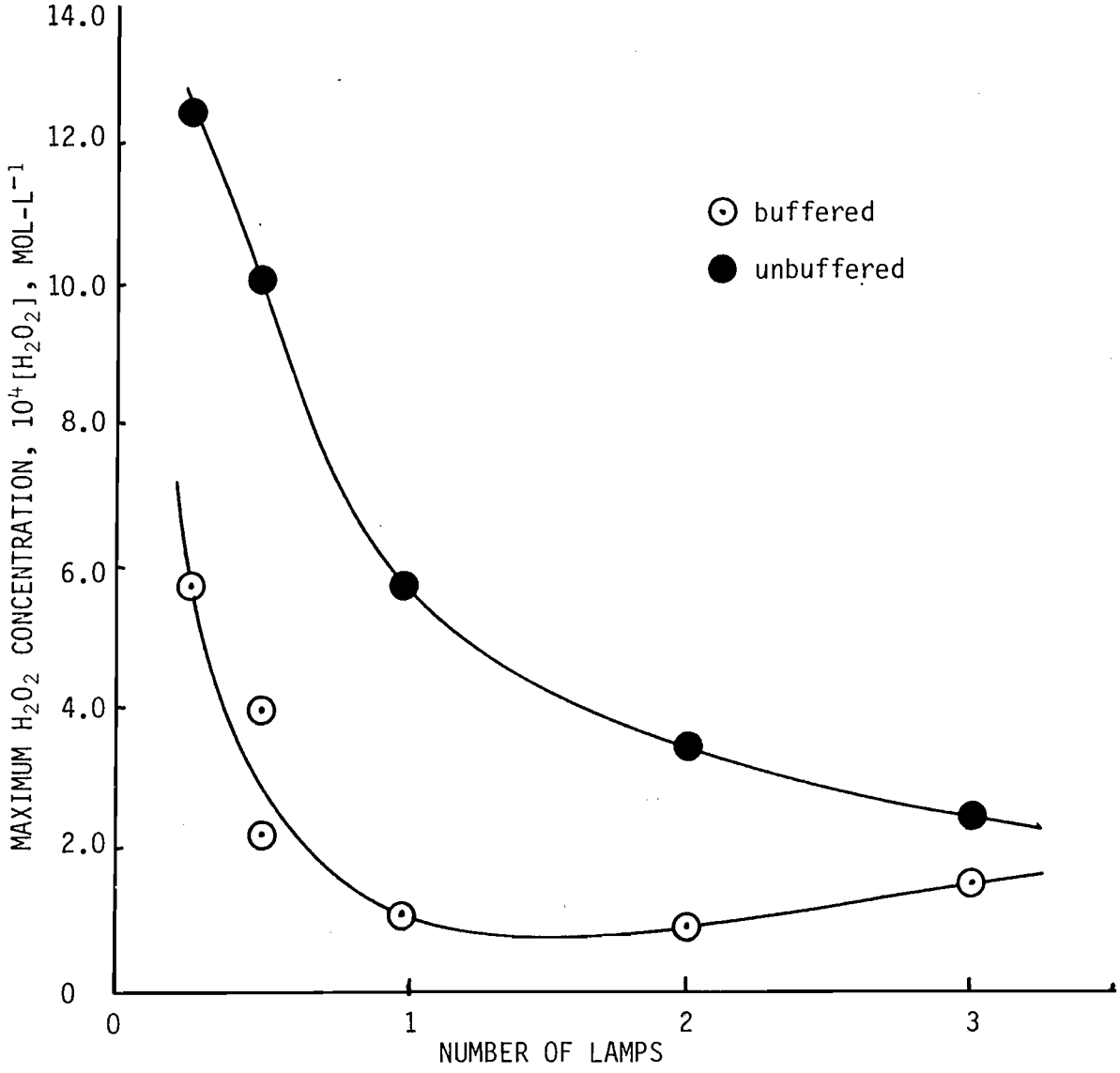

Figure 15. Maximum hydrogen peroxide concentration during methanol experiments.

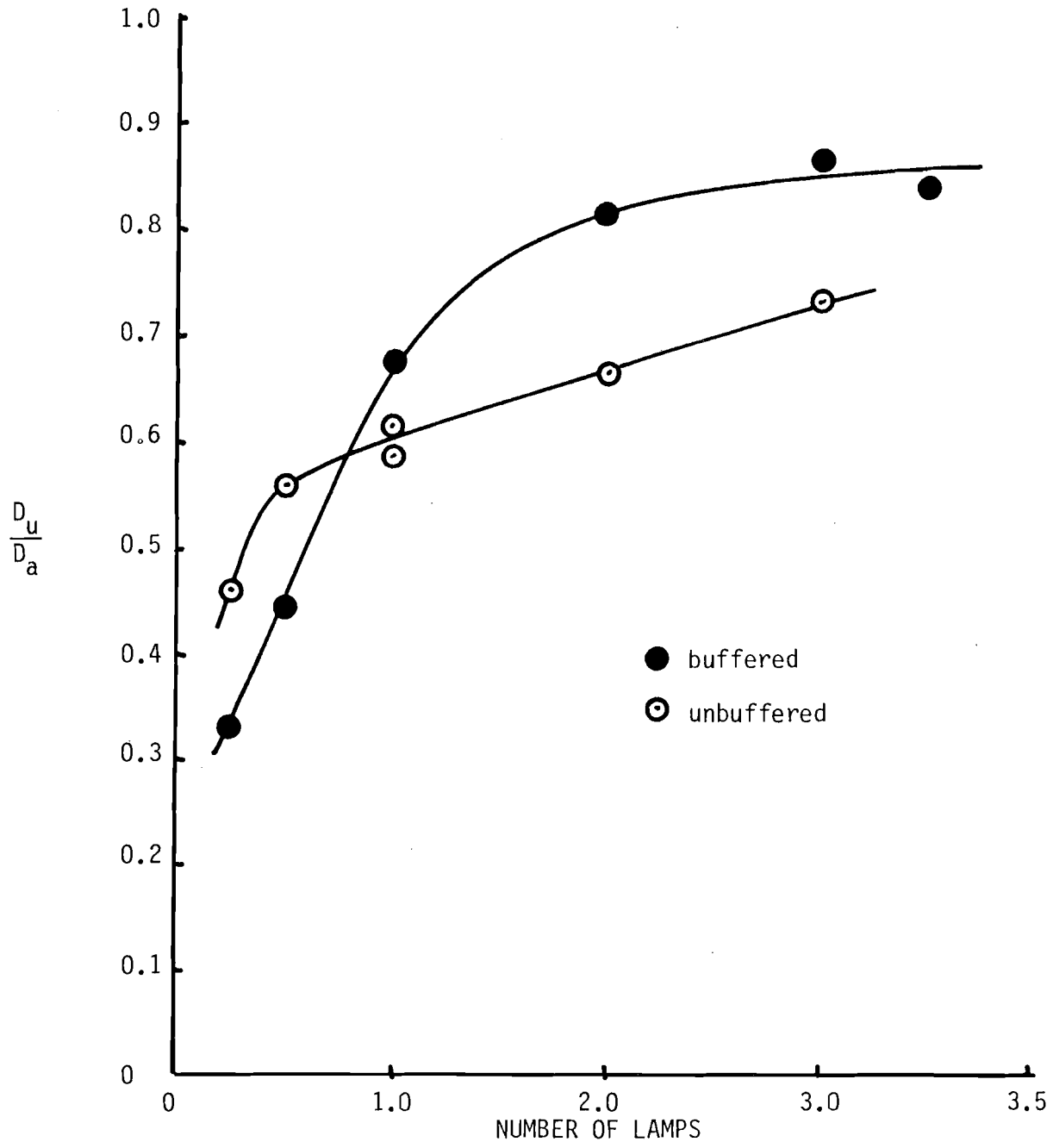

Figure 16. Ozone capture efficiency.

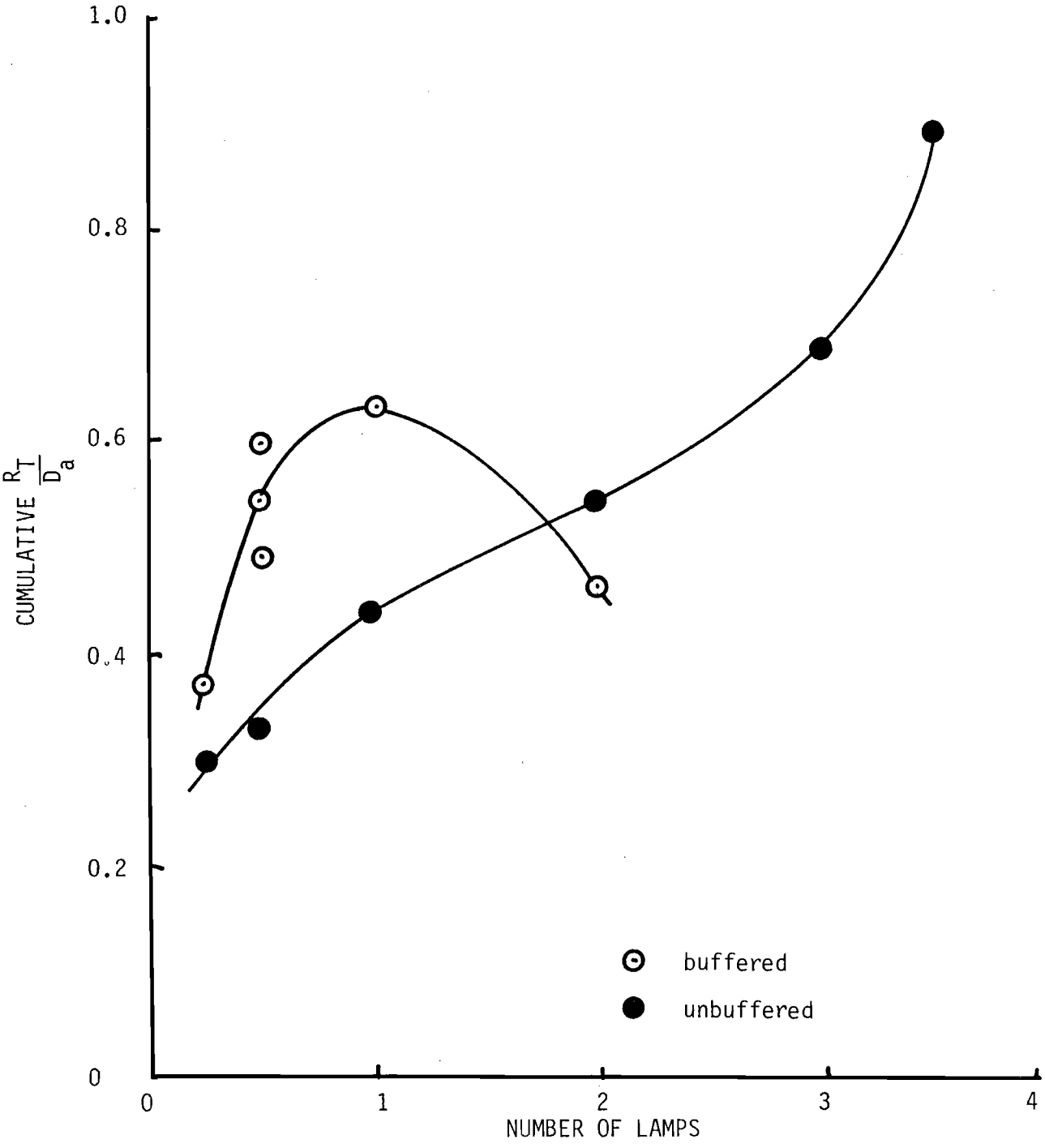

Figure 17. Utilization efficiency based on applied ozone dose rate.

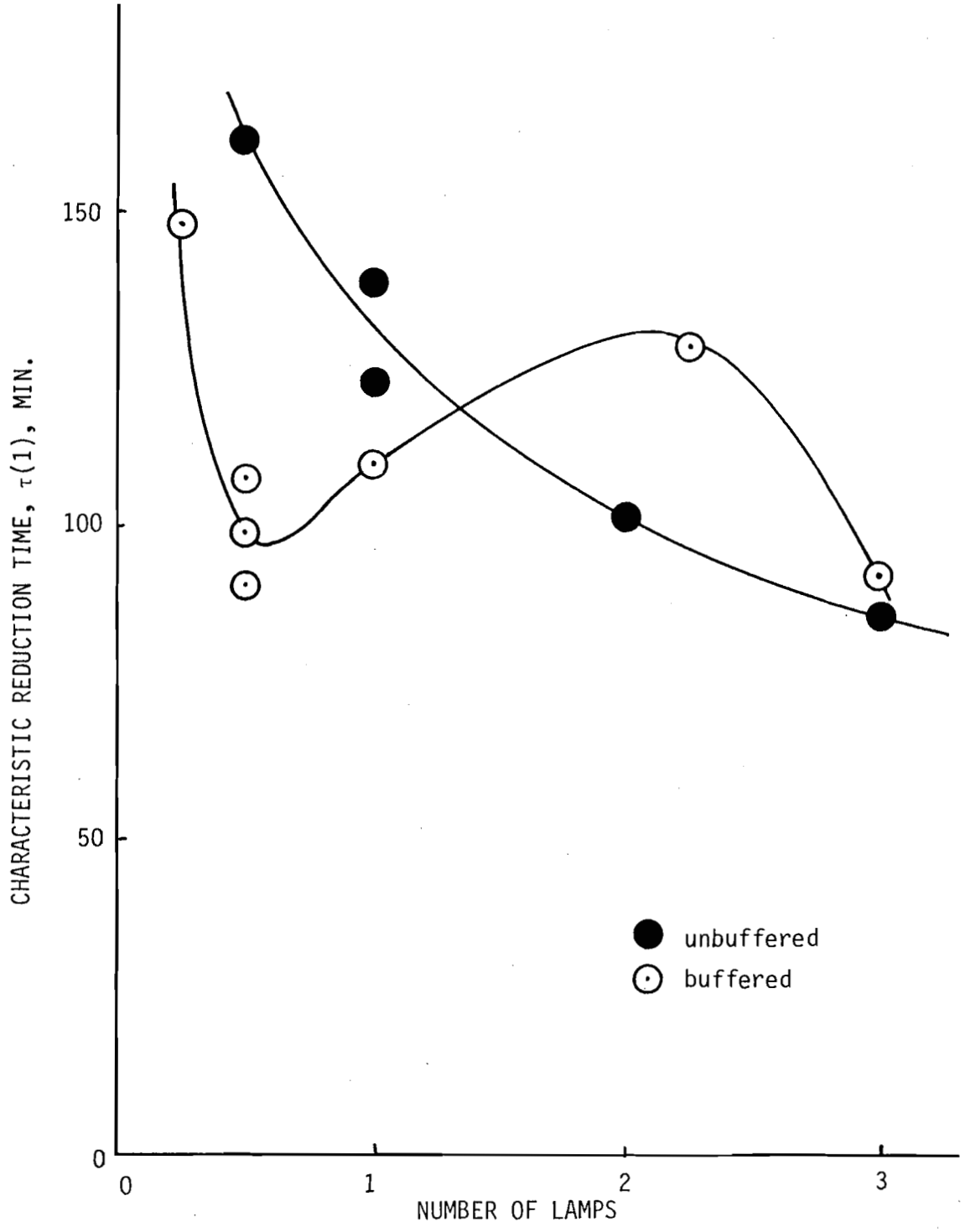

Figure 18. Characteristic substrate reduction time, $\tau(1)$, as a function of UV intensity.